

EVERY BCG WITH A STRONG RADIO AGN HAS AN X-RAY COOL CORE

M. SUN

Department of Astronomy, University of Virginia, P.O. Box 400325, Charlottesville, VA 22904-4325; msun@virginia.edu

Draft version October 20, 2021

ABSTRACT

Radio AGN feedback in cool cores has been proposed as a crucial ingredient in the evolution of baryonic structures. However, it has long been known that strong radio AGN also exist in noncool core clusters, which brings up the question whether a cool core is always required for radio feedback. In this work, we present a systematic analysis of BCGs and strong radio AGN in 145 groups and clusters from the *Chandra* archive. All 65 BCGs with radio AGN more luminous than $2 \times 10^{23} \text{ W Hz}^{-1}$ at 1.4 GHz are found to have X-ray cool cores. The BCG cool cores can be divided into two classes, the large-cool-core (LCC) class and the corona class. Small coronae, easily overlooked at $z > 0.1$, can trigger strong heating episodes in groups and clusters, long before large cool cores are formed. Strong radio outbursts triggered by coronae may destroy embryonic large cool cores and thus provide another mechanism to prevent formation of large cool cores. However, it is unclear whether coronae are decoupled from the radio feedback cycles as they have to be largely immune to strong radio outbursts. Our sample study also shows no groups with luminous cool cores ($L_{0.5-2\text{keV}} > 10^{41.8} \text{ ergs s}^{-1}$) hosting strong radio AGN with $L_{1.4\text{GHz}} > 10^{24} \text{ W Hz}^{-1}$, which is not observed in clusters. This may point to a greater impact of radio heating on low-mass systems than clusters. Few $L_{1.4\text{GHz}} > 10^{24} \text{ W Hz}^{-1}$ radio AGN ($\sim 16\%$) host a $L_{0.5-10\text{keV}} > 10^{42} \text{ ergs s}^{-1}$ X-ray AGN, while above these thresholds, all X-ray AGN in BCGs are also radio AGN. As examples of the corona class, we also present detailed analyses of a BCG corona associated with a strong radio AGN (ESO 137-006 in A3627) and one of the faintest coronae known (NGC 4709 in the Centaurus cluster).

Subject headings: cooling flows — galaxies: active — galaxies: clusters: general — X-rays: galaxies: clusters — X-rays: galaxies — radio continuum: galaxies

1. INTRODUCTION

The importance of AGN outflows for cosmic structure formation and evolution has been widely appreciated recently. AGN outflows may simultaneously explain the antihierarchical quenching of star formation in massive galaxies, the exponential cut-off at the bright end of the galaxy luminosity function (LF), the $M_{\text{SMBH}} - M_{\text{bulge}}$ relation and the quenching of cooling-flows in cluster cores (e.g., Scannapieco et al. 2005; Begelman & Nath 2005; Croton et al. 2006; Best et al. 2006). Outflows from radio AGN are especially important locally because nearly all strong radio AGN are hosted by early-type galaxies that dominate the high end of the LF and the galaxy population in clusters. Radio AGN are different from emission-line AGN selected in optical surveys. Kauffmann et al. (2004) showed that optical emission-line AGN favor low-density environments and are mainly produced by BHs with masses below $10^8 M_{\odot}$. On the other hand, radio-loud AGN favor denser environments than do normal galaxies, and the integrated radio luminosity density comes from the most massive BHs (Best et al. 2005). Best et al. (2005) also showed that the fraction of galaxies that are radio AGN increases with the stellar or BH mass (as $M_{*}^{2.5}$ or $M_{\text{BH}}^{1.6}$), while Shabala et al. (2008) found a similar relation as $M_{*}^{2.1 \pm 0.3}$ or $M_{\text{BH}}^{1.8 \pm 0.5}$. The analysis by Best et al. indicates no correlation between radio and optical emission-line luminosities for radio AGN, and the probability that a galaxy of given mass is radio loud is independent of whether it is an optical AGN. These results drove Best et al. (2005) to suggest that low-luminosity radio AGN (FR I or fainter) form a distinctly different group from optical emission-line AGN. They suggested that the radio AGN activity is associated with cooling of gas from the hot halos surrounding elliptical galaxies and clusters (see also Hardcastle et al. 2007). A similar idea

has been proposed by Croton et al. (2006). Besides the classical “quasar mode” in AGN feedback, they introduced a “radio mode” which is the result of the X-ray gas accretion on to the central BHs. The inclusion of this “radio mode” in their simulations allows suppression of both excessive cooling and growing of very massive galaxies. It also explains why most massive galaxies are red bulge-dominated systems containing old stars.

Radio activity of galaxies is enhanced in clusters and the distribution of cluster radio AGN is highly concentrated (e.g., Lin & Mohr 2007; Best et al. 2007). Among all cluster galaxies, the brightest cluster galaxy (BCG) is generally the most massive galaxy and has the biggest impact on the surrounding large cool core and the general ICM properties. With the SDSS C4 cluster sample, Best et al. (2007) found that BCGs are more likely to host a radio AGN than other galaxies of the same stellar or BH mass (see also Lin & Mohr 2007). This difference implies that either BCGs stay in each radio active cycle for a longer time, or they are more frequently re-triggered than non-BCGs. The mutual interaction between radio AGN (especially those of BCGs) and the surrounding ICM has a significant impact on both of them. The great power of jets from radio AGN can not only quench cooling in cluster cool cores, but also can drive the ICM properties away from those defined by simple self-similar relations involving only gravity (summarized in Voit 2005). The ICM around the radio AGN provides a historical chronicle of the SMBH activity. X-ray cavities and shocks serve as calorimeters for the total energy outputs of AGN that allow us to understand a great deal of AGN feedback and SMBH growth (summarized by McNamara & Nulsen 2007). On the other hand, Radio AGN (FR-I or fainter) may need an enhanced X-ray atmosphere to fuel them. Churazov et al. (2005) used Galactic X-ray binaries as analogue

for the different evolution states of the SMBH, from radiative efficient mode with weak outflows (quasars) to radiative inefficient mode with strong outflows (local giant ellipticals). The SMBHs of local giant ellipticals have very low accretion rates and radiative efficiencies, but are very efficient to heat the surrounding gas. Allen et al. (2006) presented a tight correlation between the Bondi accretion rate and the mechanical power of radio AGN for BCGs in 9 groups and clusters. The relation implies that 1% - 4% of mass energy of the gas accreted through Bondi accretion is transferred to the feedback energy to heat the surrounding ICM. Hardcastle et al. (2007) further suggested that accretion of hot gas is sufficient to power all low-excitation radio AGN (FR-I and some FR-II), while the high-excitation FR-II AGN are powered by accretion of cold gas.

As $\dot{M}_{\text{Bondi}} \propto M_{\text{BH}}^2 K^{-1.5}$ (K is entropy of the surrounding gas defined as $kT/n_e^{2/3}$), strong radio AGN require low-entropy circum-nuclear gas and massive black holes. Although many groups and clusters have large and dense cool cores (e.g., $\sim 50\%$ in the HIFLUGCS sample, Chen et al. 2007), most cluster galaxies (including many BCGs) are not located such cool cores. Their surrounding ICM has too high an entropy (> 50 times the value at the center of cluster cool cores) to trigger any significant nuclear activity. Thus, the emerging significant questions are: What fuels the strong radio AGN in groups and clusters, especially those not in large cool cores? Is an X-ray cool core always required for strong radio AGN in groups and clusters? Is the sufficient hot gas supply the reason that BCGs stay in the radio active phase longer? The work mentioned in the last two paragraphs only discussed optical and radio data of radio AGN. *Chandra* and XMM-Newton allow detailed studies of the X-ray atmosphere around radio AGN in groups and clusters. Small X-ray thermal halos around the nuclei of strong radio AGN are often found (e.g., Hardcastle et al. 2001 on 3C 66B; Hardcastle et al. 2002 on 3C 31; Worrall et al. 2003 on NGC 315; Hardcastle et al. 2005 on 3C296; Sun et al. 2005b on NGC 1265; Evans et al. 2006 on a sample of FR-I and FR-II galaxies). Hardcastle et al. (2007) also summarized some recent *Chandra* and XMM-Newton results for the hot gas atmosphere of nearby radio galaxies but the sample with detailed studies is small and those radio AGN are mainly in groups. With different original motivations, Sun et al. (2007, S07 hereafter) presented a systematic analysis of X-ray thermal coronae of early-type galaxies in 25 hot ($kT > 3$ keV), nearby ($z < 0.05$) clusters, based on *Chandra* archival data. Small and cool galactic coronae ($\lesssim 4$ kpc in radius and $kT=0.5$ -1.1 keV generally) have been found to be common, $> 60\%$ in $L_{\text{Ks}} > 2 L_*$ galaxies. Although much smaller and fainter than the classical cluster cool cores like those in Perseus, Virgo and A478, they are in fact mini-versions of large cool cores (with cooling time of 10 Myr - 1 Gyr from the center to the boundary), composed of the ISM gas (from the stellar mass loss) pressure confined by the surrounding ICM. These small coronae managed to survive strong ICM stripping, evaporation, rapid cooling, and powerful AGN outflows (see S07 for detailed discussions). One interesting result noticed by S07 is the connection between strong radio AGN and small coronae (Section 4.4 of S07). However, the S07 sample size is small (9 galaxies with $L_{1.4\text{GHz}} > 10^{24} \text{ W Hz}^{-1}$) and only small coronae were discussed. Sun et al. (2009, S09 hereafter) added six more examples of BCG coronae with strong radio AGN but the combined sample with S07 is still small. The questions raised early need to be addressed with a bigger sample. In this work, we present

results on such a sample from the *Chandra* archive (178 galaxies from 145 groups and clusters, including all BCGs, 70 galaxies with $L_{1.4\text{GHz}} > 10^{24} \text{ W Hz}^{-1}$). The plan of this paper is as follows: The galaxy sample is defined in Section 2. The data analysis is presented in Section 3, as well as the definition of cool cores in this work. In Section 4, we discuss the X-ray gas atmosphere of BCGs and non-BCGs with luminous radio AGN from the sample study. After learning the general properties of the sample, we present a detailed analysis of a luminous corona associated with a strong radio AGN in Section 5 (ESO 137-006). Many *Chandra* data are shallow so only upper limits of coronal emission exist in some cases. In Section 6, we discuss the faintest corona known that sheds light on the properties of faint embedded coronae. Discussions are in Section 7 and Section 8 contains the conclusions. We assumed $H_0 = 71 \text{ km s}^{-1} \text{ Mpc}^{-1}$, $\Omega_M=0.27$, and $\Omega_\Lambda=0.73$.

2. THE SAMPLE

We want to examine the X-ray gas component associated with BCGs and other strong radio AGN, either large cool cores or small coronae. The typically small luminosity of a corona ($\sim 10^{41} \text{ ergs s}^{-1}$ in the 0.5 - 2 keV band) limits our studies to local systems. S07 only studied $kT > 3$ keV clusters at $z < 0.05$. In this work, we include any *Chandra* observations of $z < 0.065$ groups and clusters with an exposure of longer than 5 ks. We also include higher redshift systems with sufficient *Chandra* data, but with a hard limit of $z \lesssim 0.11$. As we want to cover more volume in a single group or cluster, we limit our sample to $z > 0.01$ systems. There are very few strong radio AGN in $z < 0.01$ groups and clusters anyway. The group and cluster sample is collected from the *Chandra* archive. Two X-ray flux-limited samples, B55 (Peres et al. 1998) and HIFLUGCS (Reiprich & Böhringer 2002), are almost 100% covered by *Chandra*. However, both samples are not big and have few or no groups. As less than 1/3 of the REFLEX and NORAS clusters (Böhringer et al. 2000; Böhringer et al. 2004) have *Chandra* data, we are forced to include as many systems from the archive as we can. The final sample includes 145 groups and clusters (Table 1). Most conclusions of this work should not be much affected by the heterogeneous nature of the cluster sample. We will also discuss the B55 and the extended HIFLUGCS samples in Section 7.4.

Our main goal is to examine the X-ray gas atmosphere around BCGs so all BCGs are included in the galaxy sample. The BCG is defined as the most luminous galaxy in the 2MASS K_s band within $0.1 r_{500}$ of the group or cluster. In relaxed groups and clusters, the selection of BCGs is easy. In nine unrelaxed groups and clusters, two BCGs with comparable K_s -band luminosities are selected, including Coma, A2147, A1367, A1142, A3128, RXC J1022.0+3830, SC1329-313, A1275 and A2384. Therefore, the BCG sample includes 154 galaxies. We also want to include all galaxies with a 1.4 GHz luminosity higher than $10^{24} \text{ W Hz}^{-1}$ ($L_{1.4\text{GHz,cut}}$). A radio spectral index of -0.8 is assumed in the small radio K -correction. This $L_{1.4\text{GHz,cut}}$ is about 1/3 of the L_* of the radio luminosity function (Best et al. 2005) and is comparable to the luminosities of many nearby 3C or PKS radio galaxies. For comparison, the central radio galaxy of the Centaurus cluster (NGC 4696, PKS 1245-41) has an $L_{1.4\text{GHz}}$ of $0.60 \times 10^{24} \text{ W Hz}^{-1}$. The giant radio galaxy in our backyard, Centaurus A, has an $L_{1.4\text{GHz}}$ of $0.46 \times 10^{24} \text{ W Hz}^{-1}$. The chosen $L_{1.4\text{GHz,cut}}$ corresponds to an average mechanical power of $\sim 6 \times 10^{43} \text{ ergs s}^{-1}$ (but with large scatter, Bîrzan et

al. 2008), which is capable of increasing the thermal energy of a $10^{11} M_{\odot}$ gas core (typical for the cool cores of luminous groups and poor clusters) at $kT=1$ keV by $\sim 40\%$ in 100 Myr. For a small corona with a total gas mass of $\sim 10^8 M_{\odot}$ (S07), this kind of radio outbursts will easily destroy the whole corona if only $\sim 1\%$ of the total mechanical power is deposited within the corona for 10^8 yr. The radio fluxes come from the NRAO VLA Sky Survey (NVSS) (Condon et al. 1998) and the Sydney University Molonglo Sky Survey (SUMSS) (Bock, Large & Sadler 1999). We also examine the higher resolution images from the Faint Images of the Radio Sky at Twenty Centimeters (FIRST) survey (Becker, White & Helfand 1995) and literature if available. The origins of radio sources can be determined in all cases. Because of the proximity, spectroscopic redshifts are available for all radio galaxies in our sample. We generally use the system redshift (Table 1) to calculate distance. For the Centaurus cluster and the NGC 7619 group, we used their surface-brightness-fluctuation distance from Tonry et al. (2001).

Radio AGN are over-represented in our BCG sample. There are 50% of BCGs (77 out of 154) with $L_{1.4\text{GHz}} > 10^{23} \text{ W Hz}^{-1}$ and 32% of BCGs (49 out of 154) with $L_{1.4\text{GHz}} > 10^{24} \text{ W Hz}^{-1}$. Lin & Mohr (2007) derived the radio active fractions of BCGs for 573 groups and clusters selected from the NORAS and REFLEX cluster catalogs. Their fractions at these two thresholds are 33% and 20% respectively. von der Linden et al. (2007) and Best et al. (2007) examined a sample of 1106 groups and clusters optically selected from SDSS. The radio active fraction of BCGs is $\sim 30\%$ at $L_{1.4\text{GHz}} > 10^{23} \text{ W Hz}^{-1}$, for the typical stellar mass of BCGs in our sample. This fact again demonstrates the heterogeneous nature of our sample, which should be kept in mind when our results are interpreted. In fact, radio AGN are also over-represented in the B55 sample and the extended HIFLUGCS sample (Section 7.4). The radio AGN fractions of BCGs in these two samples are similar to ours, $\sim 50\%$ for $L_{1.4\text{GHz}} > 10^{23} \text{ W Hz}^{-1}$ AGN and $\sim 30\%$ for $L_{1.4\text{GHz}} > 10^{24} \text{ W Hz}^{-1}$ AGN. As X-ray flux-limited samples, the over-abundance of radio AGN of BCGs in both samples is mainly caused by the prevalence of large cool core clusters in both samples, as strong radio AGN are more likely to be associated with luminous cool core clusters (see Section 4).

3. THE *Chandra* DATA ANALYSIS AND THE COOL CORE DEFINITION

All observations were performed with the *Chandra* Advanced CCD Imaging Spectrometer (ACIS). Standard data analysis was performed which includes the corrections for the slow gain change¹ and charge transfer inefficiency (for both the FI and BI chips). We investigated the light curve of source-free regions (or regions with a small fraction of the source emission) to identify and exclude time intervals with strong particle background flares. We corrected for the ACIS low-energy quantum efficiency (QE) degradation due to the contamination on ACIS's optical blocking filter², which increases with time and is positionally dependent. The dead area effect on the FI chips, caused by cosmic rays, has also been corrected. We used CIAO3.4 for the data analysis. The calibration files used correspond to *Chandra* calibration database (CALDB) 3.5.2 from the *Chandra* X-ray Center. In the spectral analysis, a lower energy cut of 0.4 keV is used to minimize the effects of calibration uncertainties at low energy. The solar photospheric abundance

table by Anders & Grevesse (1989) is used in the spectral fits. Uncertainties quoted in this paper are 1σ . Special data analysis related to ESO 137-006 is discussed in Section 5.1.

In this work, X-ray cool cores include both large cool cores and small coronae. We define a large cool core if the central isochoric cooling time is less than 2 Gyr. The X-ray luminosity of a large cool core is measured within a radius where the gas isochoric cooling time is 4 Gyr ($r_{4\text{Gyr}}$). The cooling time profiles come from Sun et al. (2009), Cavagnolo et al. (2009) and our own work. Note that $r_{4\text{Gyr}}$ effectively means the whole region for a small corona (S07 and Section 5). Reasons behind these thresholds of cooling time are as follows. First, there are systems with central cooling time between 1 Gyr and 10 Gyr, or weak-cool-core clusters (e.g., Mittal et al. 2009; Pratt et al. 2009; Cavagnolo et al. 2009). Some weak cool cores also have a BCG corona, e.g., A3558 with an ICM central cooling time of ~ 4 Gyr (S07), A1060 with an ICM central cooling time of ~ 3.6 Gyr (Yamasaki et al. 2002) and A2589 with an ICM central cooling time of ~ 2.5 Gyr beyond the central source (this work). We want to select a cut of the central cooling time that excludes these sources so 2 Gyr is chosen. Systems with central cooling time of < 1 Gyr are usually considered as strong cool cores (e.g., Mittal et al. 2009; Pratt et al. 2009). Our threshold of 2 Gyr includes some weak cool cores, but not many. There are seven clusters in this sample with a central cooling time of 1 - 2 Gyr, A3571, A2244, A2063, A2142, A4038, A1650 and A2384 (north). None of them has a BCG corona (likely already merged with the large ICM cool core) and their radio AGN are always faint ($L_{1.4\text{GHz}} < 6 \times 10^{22} \text{ W Hz}^{-1}$). Thus, all large cool cores with $L_{1.4\text{GHz}} > 2 \times 10^{23} \text{ W Hz}^{-1}$ in this work are strong cool cores with a central cooling time of $\lesssim 1$ Gyr (see Section 4). Second, we want these two thresholds not too close to reflect the still high luminosities of the weak cool cores, but also not too far to have many systems fall between two thresholds. Thus, 4 Gyr is chosen as the aperture for the luminosity measurement. A somewhat different cooling time (3 - 5 Gyr) does not affect any conclusions of this work. There are seven systems in this “grey” area with a central cooling time of 2 - 4 Gyr, including A2589, A2657, A3558, A1060, AS405, A3266 and A3562. Based on our definition, they are not large cool cores so any cool cores associated with their BCGs can only be small coronae, which indeed is the case for some of them (A3558, A1060 and A2589). AS405 has the most luminous radio AGN in this group with a $L_{1.4\text{GHz}}$ of $1.65 \times 10^{23} \text{ W Hz}^{-1}$, while the radio AGN with other BCGs are all fainter than $3 \times 10^{22} \text{ W Hz}^{-1}$. As our focus is on BCGs with strong radio AGN, the exact classification of these systems in the “grey” area have little impact on our conclusions. In fact, we can conclude that weak cool cores do not have strong radio AGN, unless a corona is present.

Section 3 of S07 detailed the analysis on the identification of faint thermal sources. We always perform a spectral analysis. Most sources studied in this work have sufficient counts for a detailed spectral analysis. However, there are faint sources (e.g., with less than 90 counts in the 0.5 - 2 keV band) so the significance of the iron L-shell hump or the “softness” of the spectrum needs to be tested (see Section 3 of S07). We used the S07 method with Monte-Carlo simulations (Section 3.1 of S07) to address the significance of the iron L-shell hump. Only sources with an iron L-shell hump that is more significant at $> 99.5\%$ level are considered thermal coronae. For faint sources

¹ <http://cxc.harvard.edu/contrib/alexey/tgain/tgain.html>

² <http://cxc.harvard.edu/cal/ACIS/Cal-prods/qeDeg/index.html>

that do not meet the above criteria, we further identified “soft X-ray sources” with a power law fit as defined in Section 3.2 of S07. The power law index method is similar to the 1.5 - 7 keV / 0.5 - 1.5 keV hardness ratio method, as coronae should have strong excess emission above the continuum in the 0.5 - 1.5 keV band. As argued in S07, most “soft X-ray sources” identified by the power law index method should be genuine coronae. In fact, after the S07 work, deeper *Chandra* data for A3627 and A2052 had been available. The data cover three sources identified as “soft X-ray sources” by S07, ESO 137-008 in A3627, CGCG 049-092 and PGC 093473 in A2052 (Table 2 of S07). The deeper data clearly reveal a significant iron L-shell hump in each spectrum and confirm the corona nature for all of them. This work identified 71 small coronae. Only seven of them are flagged as “soft X-ray sources” that are not as robust as others (five in Table 2). Thus, this uncertainty has little impact on the conclusions of this work. We emphasize that the number of coronae shown in this work is only a lower limit, as *Chandra* exposures are not optimized for studies of faint galactic emission. About 2/3 of galaxies only with upper limits of coronal emission are detected in X-rays. They are either faint sources or very bright X-ray AGN that makes the identification of thermal emission difficult (see e.g., 3C 264 in S07 as an example). Different from S07, we also did not use any stacking and always studied the spectrum of a single galaxy. As shown in Section 6, the faintest embedded corona known has an X-ray luminosity much lower than any upper limits in this work. We also emphasize that the immediate local background is always used so any residual emission related to stars (LMXBs and emission from coronally active stars, see the third paragraph of Section 6) is small. We always include a power-law component in the spectral fits so the nuclear and LMXB emission is excluded.

4. RADIO AGN AND X-RAY COOL CORES

We first examine BCGs in the $L_{0.5-2\text{keV}}$ ($r < r_{4\text{Gyr}}$) - $L_{1.4\text{GHz}}$ plane (Fig. 1). BCGs in groups ($kT < 2$ keV), poor clusters ($2 \text{ keV} < kT < 4$ keV) and rich clusters ($kT > 4$ keV) are color-coded. The system temperatures come from BAX³, S09, Cavagnolo et al. (2009) and our own work. As shown in Fig. 1, almost all cool cores (including upper limits) can be divided into two classes, marked by a vertical ellipse for small coronae and a tilted ellipse for large cool cores. The dividing line between the two classes is $L_{0.5-2\text{keV}} \sim 4 \times 10^{41} \text{ ergs s}^{-1}$. The gap between two classes is especially significant at $L_{1.4\text{GHz}} > 2 \times 10^{23} \text{ W Hz}^{-1}$. There are 49 radio sources with $L_{1.4\text{GHz}} > 10^{24} \text{ W Hz}^{-1}$ and 77 radio sources with $L_{1.4\text{GHz}} > 10^{23} \text{ W Hz}^{-1}$. Above $L_{1.4\text{GHz}} > 2 \times 10^{23} \text{ W Hz}^{-1}$, **every** BCG has a confirmed cool core, small or large. In fact, there are only two non-detections of cool cores out of 77 BCGs above $L_{1.4\text{GHz}}$ of $10^{23} \text{ W Hz}^{-1}$, which is the dividing line between the star-formation and AGN components in the local radio LF (e.g., Sadler et al. 2002). Below that threshold, radio emission from star formation begins to dominate the local radio LF. This threshold was also used in the statistical studies by Lin & Mohr (2007) and von der Linden et al. (2007). Upper limits of both non-detections (AS405 and A2572) are high (Fig. 1) as both observations are short (7.9 ks) with ACIS-I, especially for AS405 at $z=0.0613$. A faint soft X-ray point source is actually detected in the position of A2572’s BCG ($z=0.0403$) but was rejected as a corona as the error of the power law index is too large (S07; Section 3). Thus, the current data are consistent with the conclusion that all BCGs with

$L_{1.4\text{GHz}} > 10^{23} \text{ W Hz}^{-1}$ have a cool core, small or large. BCGs with small coronae often host radio AGN as luminous as those BCGs in large cool cores. We call these two classes the large-cool-core (LCC) class and the corona class. The cool cores in the LCC class are the cool cores that were generally referred in the cluster papers. The corona class defined by this work also includes ~ 5 systems with small cool cores (up to 25 kpc in radius) but larger than typical coronae (less than 5 kpc in radius generally). We present the properties of the X-ray sources associated with $L_{1.4\text{GHz}} > 10^{24} \text{ W Hz}^{-1}$ radio AGN in the corona class in Table 2 (also including non-BCGs). Some examples of BCG coronae associated with strong radio AGN are also shown in Fig. 2 and 3.

4.1. The LCC class

As shown in Fig. 1, the LCC class presents an intriguing correlation between the cool core luminosity and the radio luminosity of the BCG, unlike the corona class. More luminous cool cores generally host more luminous radio sources, although the scatter is large. From the BCES Orthogonal fit (Akritas & Ber-shady 1996), $L_{1.4\text{GHz}} \propto L_X^{1.91 \pm 0.20}$. Why does this correlation exist for the LCC class? It is not clear that this is related to radio feedback. On the other hand, environmental radio boosting can tilt the LCC class to the observed trend, as more luminous cool cores are generally bigger and are more capable to confine the radio lobes to stop adiabatic expansion (e.g., Barthel & Arnaud 1996; Parma et al. 2007). Radio lobes can then be brighter and exist for a longer life time. Thus, it is necessary to re-produce Fig. 1 for the radio nuclei, jets and lobes separately. However, the relevant data are not available for most radio AGN in this sample. We leave the question of the tilted LCC class to future work as the corona class is the focus of this work.

The most intriguing result in Fig. 1 is for galaxy groups. There are 19 groups with a cool core that is more luminous than $6 \times 10^{41} \text{ ergs s}^{-1}$, but none of them hosts a $L_{1.4\text{GHz}} > 10^{24} \text{ W Hz}^{-1}$ AGN. Even at a lower radio luminosity threshold ($3 \times 10^{23} \text{ W Hz}^{-1}$), groups in the corona class outnumber groups in the LCC class by 17 to 1, while there are in fact less cluster BCGs in the corona class than the LCC class (16 versus 27). This deficiency of high $L_{1.4\text{GHz}}$ groups in the upper portion of the LCC class is not observed in clusters. Two local systems ignored in our sample (but included in the B55 and the HIFLUGCS-E samples, see Section 7.4), the Virgo cluster and the Fornax cluster, also fit into this picture. The Virgo cluster hosts a $L_{1.4\text{GHz}} = 5.3 \times 10^{24} \text{ W Hz}^{-1}$ AGN in the center but its temperature is ~ 2.3 keV (e.g., Shibata et al. 2001). The central radio source in the Fornax cluster is faint ($L_{1.4\text{GHz}} = 3.2 \times 10^{22} \text{ W Hz}^{-1}$). Is the deficiency of luminous group cool cores with a strong radio AGN a selection bias from the heterogeneous nature of our sample? Nearby groups are observed by *Chandra* either because they are bright or they host bright central radio galaxies (so selected by the AGN panels). Groups are then likely under-represented in the lower portion of the corona class, but they are much less likely to be missed in the upper portion of the LCC class. The absence of $L_{0.5-2\text{keV}} > 6 \times 10^{41} \text{ ergs s}^{-1}$ cool cores with a strong radio AGN for groups and poor clusters is also the reason why there is a gap between two classes at high radio luminosity. Nevertheless, this result needs to be examined with samples unbiased to the above conclusion (e.g., optically selected). If this result holds, it may point to a bigger role of radio outbursts for group gas than for cluster gas,

³ <http://bax.ast.obs-mip.fr/>

as the gas cores of groups are more vulnerable to powerful radio outbursts compared to the larger, hotter gas cores of clusters.

4.2. The corona class

The properties of embedded coronae have been presented and discussed in detail by S07. Jeltima et al. (2008) presented a similar analysis on coronae in groups. We have added many more coronae for BCGs. As shown in Fig. 1, X-ray luminosities of coronae show little correlation with the radio luminosities of the galaxy, although coronae with strong radio AGN are usually luminous. As emphasized in S07 and early in this paper, small coronae in the upper portion of the corona class will be destroyed even if only $< 1\%$ of AGN heating is acted inside the corona. Being in rich environments (especially if in hot clusters), it is difficult to rebuild these mini-cool cores from stellar mass loss, once they are destroyed. S07 and this work show that very few coronae of massive galaxies should have been destroyed in this way. Powerful radio jets may simply penetrate the coronal atmosphere with very little energy deposition. However, if radio outbursts have little impact inside a small corona, is radio heating still responsible for quenching cooling inside a corona and turning off the nuclear activity? This is the same cooling/heating question in large cool cores. Compared small coronae with large cool cores, the global cooling is much weaker (but still strong in the center) while heating is not apparently different from that in large cool cores (Fig. 1). We will return to this issue in Section 7.

We also present the results for 21 non-BCGs with $L_{1.4\text{GHz}} > L_{1.4\text{GHz, cut}}$ (Fig. 4). Most non-BCGs do not have a confirmed corona but the upper limits are usually high. Section 6 presents the faintest embedded corona known (NGC 4709), which is much fainter than all upper limits in this work. We also present the $L_{\text{Ks}} - L_{0.5-2\text{keV}}$ plot for all galaxies in this work (Fig. 5). The corona class falls around the average relation derived by S07, while the cool cores in the LCC class are much X-ray brighter. We also included the expected emission from cataclysmic variables and coronally active stars (Revnivtsev et al. 2008), which is always small. As discussed in Section 6, the real contribution is even much smaller as we always used the immediate local background that also includes much stellar emission. S07 showed that massive galaxies generally have luminous coronae. There are some non-detections of coronae for massive galaxies in Fig. 5. Generally the upper limits are still high. Interestingly, above L_{Ks} of $3.5 L_{\text{Ks,*}}$ (or $10^{11.61} L_{\text{Ks},\odot}$, the dotted line in Fig. 5), the galaxies associated with $L_{1.4\text{GHz}} > 10^{23} \text{ W Hz}^{-1}$ AGN are generally more X-ray luminous than those with weak radio AGN. Massive BCGs with a moderate corona or no corona usually only have weak radio AGN. Thus, the strong connection between BCGs with strong radio AGN and X-ray cool cores is not all because of their strong correlations with the galaxy mass.

4.3. X-ray AGN vs. Radio AGN

We also examined the fraction of X-ray AGN ($L_{0.5-10\text{keV}} > 10^{42} \text{ ergs s}^{-1}$) in our sample. Fainter AGN exist in many cases (Table 2). However, the confirmation and determination of their properties are often affected by bright cluster cool cores, possible intrinsic absorption and LMXBs. Moreover, fainter X-ray AGN cannot be well studied at $z > 0.5$ anyway. The results are summarized in Table 3. There are only eleven X-ray AGN above the threshold in total: NGC 1275, Cygnus A, Hydra A, five non-BCGs in A3667, A514, A754, A2142 and A3880,

3C264 in A1367, NGC 2484 and NGC 6251 (Table 2). The fractions in all four sub-samples of Table 3 are small, although it indeeds increases in the radio AGN sample. We also notice that all BCGs with an $L_{0.5-2\text{keV}} > 10^{42} \text{ ergs s}^{-1}$ AGN host an $L_{1.4\text{GHz}} > 10^{24} \text{ W Hz}^{-1}$ radio AGN. Conversely, if a BCG hosts a radio source that is weaker than $10^{24} \text{ W Hz}^{-1}$ at the 1.4 GHz, its X-ray AGN is never more luminous than $10^{42} \text{ ergs s}^{-1}$ in this sample (154 BCGs).

5. A DETAILED CASE STUDY: ESO 137-006 IN A3627

The last section has depicted the general properties of the corona class. How does a BCG corona associated with a luminous radio AGN look in detail? In this section we present a detailed analysis of a BCG corona with a strong radio AGN, ESO 137-006 in A3627. ESO 137-006 is the brightest (not the most luminous) embedded corona in $kT > 3 \text{ keV}$ clusters (S07), because of its proximity. A new 57.3 ks ACIS-S observation collects about 3800 source counts in the 0.5 - 3 keV band ($\sim 96\%$ from the gas). Before this observation, NGC 3842 in A1367 (Sun et al. 2005a) had the most *Chandra* counts (~ 1000 from a 43.2 ks ACIS-S observation) for an embedded corona. Other coronae discussed in the literature (e.g., Coma, Vikhlinin et al. 2001; NGC1265 in Perseus, Sun et al. 2005b) only have ~ 500 counts typically. In fact, even including groups and poor clusters, only IC 4296 and NGC 315 have brighter coronae. However, both are in poor groups so the surrounding ICM has a comparable temperature. Both also host bright nuclear sources and there is a bright X-ray jet in NGC 315 (Worrall et al. 2003), which causes some trouble for the analysis of the X-ray gas. Radio AGN associated with these two galaxies are > 17 times fainter than ESO 137-006's. Thus, ESO 137-006 is the best case of a luminous corona associated with a strong radio AGN for a detailed analysis. In S07, we present the results from an 14.1 ks ACIS-I observation targeted on a cluster position that is $5'$ from ESO 137-006. Here we present the results from a much deeper targeted ACIS-S observation in cycle 8 (PI: Sun).

At $z = 0.01625$ (Woudt et al. 2007), A3627 ($kT \sim 6.5 \text{ keV}$) is the closest massive cluster. It is also the sixth brightest cluster in RASS and the second brightest non-cool-core cluster after Coma (Böhringer et al. 1996). ESO 137-006 is the BCG of A3627. ESO 137-008 (also with a small corona) has the same K_s band magnitude as ESO 137-006's, but its velocity dispersion is much smaller (see Table 2 of S07). The radio WAT source associated with ESO 137-006, PKS 1610-60 (Jones & McAdam 1996), is one of the brightest radio sources in the southern hemisphere and its 1.4 GHz luminosity is 53% higher than NGC 1275's (Fig. 1; Table 2). The XMM-Newton mosaic image of A3627 is shown in Fig. 6, along with the radio contours from SUMSS. One can observe evidence of the interaction between the radio lobes and the ICM in Fig. 6, which implies that ESO 137-006 is either embedded in the cluster gas core or not far from it. For the assumed cosmology (Section 1), the angular scale is $0.327 \text{ kpc / arcsec}$ and the luminosity distance of A3627 is 69.6 Mpc.

5.1. Chandra data analysis

The observation of ESO 137-006 was performed with ACIS-S on 2007 July 8. Standard *Chandra* data analysis was performed (see Section 3). No background flares were present. The effective exposure is 57.3 ks for the S3 chip. The observation was performed in the VFAINT mode. However, we only use the FAINT mode for the analysis of the corona source, as

the VFAINT filtering causes a 2% loss on the source counts, mostly at the center of the corona. We still use the VFAINT mode for the analysis the surrounding ICM. In the analysis of the corona, we also removed the pixel randomization. A Galactic absorption of $1.73 \times 10^{21} \text{ cm}^{-2}$ is used, which fits the spectra well.

5.2. The properties of the surrounding ICM

Before we study ESO 137-006's corona, the properties of the surrounding ICM were examined to constrain the ambient gas temperature and pressure. As discussed in the Appendix of S07, the soft X-ray background is high in the direction of A3627. S09 developed a method to constrain the local X-ray background with the stowed background. Following the S09 method, we derived a local soft X-ray background flux surface density of $(12.1 \pm 1.0) \times 10^{-12} \text{ ergs s}^{-1} \text{ cm}^{-2} \text{ deg}^{-2}$ in the 0.47 - 1.21 keV band. The RASS R45 flux measured from 1 - 2 deg annulus centered on A3627, excluding a bright PS, is $290 \times 10^{-6} \text{ cnts s}^{-1} \text{ arcmin}^{-2}$. These two fluxes well match their average relation shown in the Fig. 2 of S09. The hotter thermal component of the local X-ray background has a temperature of $0.33 \pm 0.03 \text{ keV}$ (see the local background model in S09), which is consistent with the trend that its temperature increases to $\gtrsim 0.3 \text{ keV}$ in the high R45 flux regions (S09).

With the local X-ray background determined, the temperature profile of the surrounding ICM was derived ($\sim 7 \text{ keV}$, Fig. 7). The ICM abundance from the joint fit of the three radial bins is 0.32 ± 0.09 solar, which is much lower than that of the small corona (the next section). The ICM electron density from the ROSAT data is $\sim 1.4 \times 10^{-3} \text{ cm}^{-3}$ at the projected position of ESO 137-006 (Böhringer et al. 1996).

5.3. The properties of ESO 137-006's corona

The 0.5 - 5 keV *Chandra* count image of ESO 137-006 is shown in Fig. 6. Beyond the bright core, the corona is more extended towards the south, which implies ESO 137-006's motion to the north. This is consistent with the small bending of its radio lobes (Fig. 6). To better show the central part of the corona, we applied the Subpixel Event Repositioning tool developed by Li et al. (2004) to the data to make the 1/4 subpixel image (the right bottom panel of Fig. 6). Within the central 0.5 kpc, the gas is flattened along the north-south direction, which is also perpendicular to the direction of the radio jets.

We derived the profiles of the X-ray surface brightness, temperature (projected and deprojected), density, entropy, cooling time and pressure for the corona, as shown in Fig. 7. In the spectral analysis, the local background is extracted from the $34'' - 120''$ (11.1 - 39.2 kpc) annulus. VAPEC was used in each annulus, as it fits the spectral lines better. We used the classical "onion-peeling" method for deprojection. For such a massive galaxy, the LMXB emission should be significant. We used the $L_{X, \text{LMXB}} - L_{K_s}$ scaling relation derived by Kim & Fabbiano (2004). As there are no *HST* data of ESO 137-006, we simply used the *HST* stellar light profile of NGC 3842 for the stellar light profile of ESO 137-006 (Sun et al. 2005a), as two BCGs have similar 2MASS K_s luminosities (0.22 mag difference). After adjusting to ESO 137-006's K_s -band luminosity and A3627's local background, one can see that the LMXB light + a flat local background well describes the observed profile beyond $\sim 4.2 \text{ kpc}$ radius. In fact, the net spectrum in the $13'' - 34''$ annulus (with the $34'' - 120''$ spectrum as the local background) can be well fitted by a power law with a photon index of

1.7. Its flux is also consistent with the expected LMXB flux in the region (Table 4). Thus, we conclude that the corona is pressure confined at $\sim 4.2 \text{ kpc}$ radius. In fact, the electron pressure ratio across the 4.2 kpc boundary is 1.57 ± 0.69 , consistent with pressure equilibrium. Obviously, there are large jumps of entropy and cooling time across the boundary. Across the coronal boundary, heat conduction has to be suppressed by a factor of at least ~ 170 from the Spitzer value, using the ratio of the heat conduction flux and the total X-ray flux (the method used in S07). Without any suppression, this small corona will be evaporated in $\sim 10 \text{ Myr}$ (S07). Inside the boundary, the corona has low entropy and short cooling time (Fig. 7). that is typical for the center of large cool cores. The properties of ESO 137-006's corona are summarized in Table 4.

As the abundances in each annulus are all consistent with the same value (from the VAPEC model), we fix them together. The best-fit abundances from the VAPEC model are listed in Table 4. We also derived the abundance ratios: $\text{Si/Fe} = 1.47^{+0.94}_{-0.58}$, $\text{Fe/O} = 2.17^{+3.60}_{-1.42}$, and $\text{Fe/Mg} = 0.50^{+0.35}_{-0.20}$. These ratios can be compared with the theoretical estimates from Iwamoto et al. (1999): $\text{Fe/O} = 0.26$, $\text{Si/Fe} = 3.03$, and $\text{Fe/Mg} = 0.26$ for SNII, $\text{Fe/O} = 27-75$, $\text{Si/Fe} = 0.54-0.62$, and $\text{Fe/Mg} = 31-69$ for SNIa. Thus, the abundances of the corona is not only enriched by SNIa.

As shown in Fig. 7, the central density is high. Can we constrain the gas properties around the Bondi radius? The mass of the central SMBH can be estimated from the K_s -band luminosity of the galaxy (Marconi & Hunt 2003, see Section 7.1), $1.61 \times 10^9 M_\odot$. The Bondi radius is then 62 pc (or $0.19''$) for a central temperature of $\sim 0.8 \text{ keV}$ (Fig. 7). This scale is unresolved. However, we can still constrain the range of gas density and entropy around the Bondi radius, from the measured total X-ray emission within the innermost bin. We assume $n_e = n_{e,0}(r/r_0)^{-\alpha}$, where r_0 is the Bondi radius and $n_{e,0}$ is the electron density at r_0 . Of course, $\alpha < 1.5$. We integrated the density model to compare with the observed X-ray luminosity within the innermost bin, assuming a constant emissivity. As shown in Fig. 8, the gas density at the Bondi radius is always $\lesssim 1.8 \text{ cm}^{-3}$, even when the PSF correction is considered. Similarly to compare the model with the emission-weight temperatures observed, we find that the gas temperature at the Bondi radius is 0.8 - 0.9 keV. These results will be used in Section 7.1 to examine whether Bondi accretion is sufficient to power the radio AGN of ESO 137-006.

In spite of its high central density, the size of ESO 137-006's corona is small so the total gas mass is very small, $(1.78 \pm 0.19) \times 10^8 M_\odot$ within $13''$ (or 4.24 kpc) radius. This can be compared with the typical gas mass within 10 Gyr cooling radius for luminous cool cores in groups and clusters, $\sim 10^{11} - 5 \times 10^{12} M_\odot$ (S09; Cavagnolo et al. 2009). Owing to the vast contrast, S07 named the embedded coronas as mini-cooling cores. As we will discuss in Section 7, this kind of mini-cooling cores is sufficient to fuel powerful FR-I radio galaxies. As shown in Fig. 1 and Table 2, the X-ray luminosity of ESO 137-006's corona is not particularly high in the corona class. Thus, we expect that other luminous BCG coronae would have similar properties to those of ESO 137-006's.

6. HOW FAINT AN EMBEDDED CORONA CAN BE?

There are upper limits of the coronal emission in Fig. 1, 4 and 5, so it is interesting to know how faint an embedded corona can be. Strong ram pressure in groups and clusters gen-

erally only allows coronae with dense cores to survive (S07). While many BCGs have luminous coronae ($L_{0.5-2\text{keV}} \sim 10^{41}$ ergs s^{-1} , Fig. 4 and 5), faint embedded coronae with moderate cool cores do exist. For BCGs associated with luminous radio AGN, the faintest corona known is the one associated with NGC 3862 (or 3C 264) in A1367 ($L_{0.5-2\text{keV}} \sim 1.4 \times 10^{40}$ ergs s^{-1} , Table 2; S07). One can see that its luminosity is comparable to or smaller than all upper limits for non-detections in this work (Fig. 4 and 5). How faint can a BCG corona be? In this section we discuss the corona of NGC 4709, which has the lowest X-ray luminosity known for an embedded corona in a galaxy more luminous than L_* .

NGC 4709 is the dominant galaxy of a shock-heated subcluster falling into the Centaurus cluster (Churazov et al. 1999). A faint corona was detected near the edge of the S1 chip in a 34.3 ks *Chandra* observation (S07). Here we present the results from our new targeted observation. We adopt a distance of 35.3 Mpc for NGC 4709 (Tonry et al. 2001), which is much smaller than the distance we used in S07 (49.4 Mpc). The angular scale is 0.167 kpc / arcsec. The observation of NGC 4709 was performed with ACIS-S on 2007 March 25. No background flares were present. The effective exposure is 29.7 ks. An extended but faint source is detected at the position of NGC 4709. A strong iron L-shell hump centered at ~ 0.9 keV clearly shows the presence of the thermal gas. The new targeted observation allows better removal of the local background. Half of the 0.5 - 2 keV counts are from a hard power-law component (likely LMXBs) and about 90 counts are from the emission of the thermal gas. The gas temperature is 0.78 ± 0.09 keV with a fixed abundance of 0.8 solar (see S07). The temperature difference from S07 comes from the different contribution of the hard power-law component in the spectral fits. The S07 fit to the old S1 data allows little flux from the hard component. The rest-frame 0.5 - 2 keV luminosity is 1.8×10^{39} ergs s^{-1} , which makes it the faintest corona known in clusters (S07 and this work). We compare its *Chandra* surface brightness profile with that of ESO 137-006 in Fig. 9. The contribution of the LMXB light has been removed, assuming that it follows the stellar light. One can see the vast difference. The corona boundary is ~ 2.0 kpc. Assuming a constant emissivity for the corona, the central electron density of the gas is 0.034 cm^{-3} and the total gas mass is $2.9 \times 10^6 M_\odot$ within a 2 kpc radius (Table 4). The central cooling time is ~ 0.13 Gyr so it is still a moderate cool core. The properties of NGC 4709's corona are summarized in Table 4 to compare with those of ESO 137-006's corona.

We indeed notice that faint thermal emission can also come from the integrated emission of cataclysmic variables and coronally active stars (e.g., Revnivtsev et al. 2008). This emission component is linearly scaled with galaxy's K_s -band luminosity (Revnivtsev et al. 2008). As shown in Fig. 5, the expected luminosity of this component gets close to that observed for NGC 4709, although it is far smaller than those of luminous coronae. However, one needs to remember that in our analysis of small coronae, local background is always used. For NGC 4709, the global spectrum is extracted from an aperture of 2.23 kpc in radius, while the local background is from the 2.23 kpc - 5.82 kpc annulus. We analyzed the 2MASS K_s band image and found that the net stellar emission within 2.23 kpc radius is only $\sim 3.5\%$ of galaxy's total light, after subtracting the local background from the 2.23 kpc - 5.82 kpc annulus. Moreover, NGC 4709's X-ray source is more peaked than the optical light. Thus, we are confident that NGC 4709 has an X-ray

gaseous halo.

Coronae like NGC 4709's are so faint that they are easily overlooked at $z > 0.03$. Coronae like 3C264's can also be easily overlooked at $z > 0.07$, especially when a bright X-ray nuclear source is present (the case for 3C264). This fact needs to be kept in mind when $z \gtrsim 0.05$ FR-I radio galaxies or cluster BCGs are studied. A significant X-ray gas component may elude detection easily.

7. DISCUSSION

7.1. Fueling radio AGN

What fuels the radio AGN in groups and clusters? We focus on radio AGN associated with a small corona, as radio AGN in the LCC class have been widely discussed in the literature. Even for small coronae, there should be sufficient amount of gas cooled from the hot phase to fuel the radio AGN. The maximum mass deposition rate from cooling (assuming steady and isobaric) is: $\dot{M}_{\text{cooling}} \approx 2\mu_{\text{mp}} L_{\text{X,bol}} / 5kT = 0.44 (L_{\text{bol}} / 10^{41} \text{ ergs s}^{-1}) (kT / 0.9 \text{ keV})^{-1} M_\odot / \text{yr}$. We calculate \dot{M}_{cooling} for each corona in the upper portion of the corona class (Fig. 10). The bolometric correction is made case by case. For upper limits, we assume a temperature of 0.7 keV (S07). The required SMBH accretion rate is estimated from the $L_{1.4\text{GHz}}$ - jet power relation by Birzan et al. (2008), assuming a mass-energy conversion efficiency of 0.1. As shown in Fig. 10, the required SMBH accretion rate is always small and there should be enough amount of cooled gas in coronae. The reality is however more complicated. First, the above cooling rate is reduced if there are heat sources. Even if strong radio outbursts deposit very little heat inside a corona, SN heating can be significant as discussed in S07. On the other hand, the stellar mass loss rate from evolved stars is significant inside coronae, 0.2 - 0.8 M_\odot / yr (Faber & Gallagher 1976; S07). However, both the SN heating and the stellar mass loss should follow the stellar light profile, which is much shallower than the X-ray emission profile of coronae (S07). The detailed energy balance and evolution of gas in different phases is unclear. However, as argued in S07, cooling in the central kpc of a luminous corona (where most X-ray emission comes from) should overwhelm heating so the actual mass deposition rate should not be reduced much from the above estimates. Second, the $L_{1.4\text{GHz}}$ - jet power relation in Birzan et al. (2008) was derived from radio AGN in the LCC class, where the radio luminosity of lobes may be enhanced by the high ICM pressure of large cool cores (e.g., Barthel & Arnaud 1996). Moreover, the Birzan et al. (2008) relation likely underestimates the jet power by missing power from undetected weak shocks and cavities. These two factors should not increase the jet power by more than a factor of a few (McNamara & Nulsen 2007) so cooling of small coronae should provide enough fuel for their radio AGN.

Are radio AGN fueled by hot gas (e.g., Best et al. 2005; Croton et al. 2006; Allen et al. 2006; Hardcastle et al. 2007)? Typically for hot accretion, Bondi accretion is assumed (e.g., Hardcastle et al. 2007). The Bondi accretion rate is: $\dot{M}_{\text{Bondi}} = 0.0042 (K / 2 \text{ keV cm}^2)^{-3/2} (M_{\text{BH}} / 10^9 M_\odot)^2 M_\odot / \text{yr}$. K is the gas entropy at the Bondi radius. The Bondi radius in this sample (10 - 150 pc) is always unresolved. However, as shown in Section 5.3, the gas entropy can still be constrained from the observed X-ray luminosity of the innermost bin. For the best-studied case, ESO 137-006, we take the gas entropy at the Bondi radius as $0.8 \pm 0.3 \text{ keV cm}^2$ (Section 5.3). There are four luminous coronae that we performed detailed studies be-

fore, NGC 3842 and NGC 3837 (Sun et al. 2005a), NGC 1265 (Sun et al. 2005b) and 3C 465 (S07). Their central entropy values are $\lesssim 1.1\text{--}1.8 \text{ keV cm}^2$. For the faintest corona of a massive galaxy, NGC 4709's corona, the central entropy is $\sim 6.5 \text{ keV cm}^2$ (Section 6). As we cannot perform a similar analysis for ESO 137-006's corona on other coronae, we simply assume an average entropy of 2 keV cm^2 , with an uncertainty range of $1\text{--}3 \text{ keV cm}^2$ (note that Hardcastle et al. 2007 used an entropy value of 1.11 keV cm^2). The SMBH mass is estimated from the 2MASS K_s band luminosity of the galaxy (Marconi & Hunt 2003), $\log(M_{\text{SMBH}}/M_\odot) = 9.47 + 1.13 \log(L_{K_s}/10^{12}L_\odot)$. The results are also shown in Fig. 10. A large Bondi accretion rate needs a massive black hole and low-entropy surrounding gas. Both requirements point to massive galaxies (recall the $L_X - L_{K_s}$ correlation for coronae, e.g., S07). Thus, low-mass galaxies with a faint corona may not power their radio AGN through hot accretion (Fig. 10), especially if the required SMBH accretion rate is higher for the reasons presented in the last paragraph. On the other hand, SMBH spin can reduce the required accretion rate (e.g., Wilson & Colbert 1995; McNamara et al. 2009).

Besides hot gas, dust and molecular gas are also present in early-type galaxies and BCGs. Dust with mass $\lesssim 10^4 - 10^5 M_\odot$ was detected in $\sim 80\%$ of nearby large early-type galaxies (e.g., van Dokkum & Franx 1995). The origin of dust includes mergers with dust-rich dwarfs and a stellar origin (Mathews & Brighenti 2003). Interestingly, the dust detection rate is higher in radio-jet galaxies than in non radio-jet galaxies (e.g., de Koff et al. 2000; Verdoes Kleijn & de Zeeuw 2005; Simões Lopes et al. 2007). For galaxies with dust detections, FR-I galaxies also have more dust than radio-quiet ellipticals. The dust in FR-I galaxies is generally situated in sharply defined disks on small ($< 2.5 \text{ kpc}$) scales, while radio jets are generally perpendicular to the dust disk (e.g., de Koff et al. 2000). Sometime the dust disk is warped (e.g., 3C 449 in our sample, Tremblay et al. 2006), likely in the process of settling down to be regular disks or are being perturbed (Verdoes Kleijn & de Zeeuw 2005). The dust-jet connection is still not understood (e.g., which impacts which?) but dust may play a role to fuel the central SMBH. There is also mounting evidence of CO detections in radio galaxies (e.g., Lim et al. 2000; Evans et al. 2005; Prandoni et al. 2007). Three galaxies in our sample belongs to this growing class, 3C 31 ($M_{\text{HI}} = 4.8 - 8.9 \times 10^8 M_\odot$, Lim et al. 2003; Evans et al. 2005), 3C 264 or NGC 3862 ($M_{\text{HI}} = 2.6 \times 10^8 M_\odot$, Lim et al. 2003) and 3C 449 ($M_{\text{HI}} = 2.4 \times 10^8 M_\odot$, Lim et al. 2003). The CO emission of 3C 31 and 3C 264 exhibits a double-horned line profile characteristic of a rapidly-rotating disk (Lim et al. 2000). At least eleven other galaxies in our sample were undetected in these CO observations, with upper limits of $(1\text{--}5) \times 10^8 M_\odot$. All these values have been adjusted to our cosmology. It is intriguing that the estimated mass values or upper limits of the HI gas are comparable or even larger than the mass values of the X-ray gas of their coronae, although the cold gas can in principle be produced through cooling over $< 1 \text{ Gyr}$. More detailed molecular data of BCGs with and without strong radio AGN will better reveal the connection between the radio activity and the cold gas component. A related question is on the nuclear star formation in small coronae. Rafferty et al. (2008) and Cavagnolo et al. (2008) showed that star formation turns on when the central cooling time of the gas falls below $\sim 0.5 \text{ Gyr}$ or the gas entropy falls below $\sim 30 \text{ keV cm}^2$ (at $r = 3\text{--}4 \text{ kpc}$ for ESO 137-006, Section 5). Will this be the

case for small coronae? On the other hand, the energy balance and transfer between gas in different phases (molecules, dust, stellar winds and $10^7\text{--}10^8 \text{ K}$ X-ray gas) is an interesting problem to explore.

To sum up, cooling of the X-ray coronae can provide enough fuel to the central SMBH, provided that the cooled materials can reach the very center. Bondi accretion may be sufficient for the massive black holes in a luminous X-ray corona, but likely not the only answer for the strong radio AGN in the corona class. Fig. 10 also does not necessarily argues for hot accretion for massive galaxies as there are many uncertainties. Besides ones mentioned above, it should be aware that a small amount of angular momentum of the hot gas can largely reduce the accretion rate (e.g., Proga & Begelman 2003). The large scatter of the $L_{1.4\text{GHz}}$ - jet power relation also implies that some strong radio AGN will require much higher mass accretion rates than the average values. On the other hand, dust and molecular gas co-exist with the $10^7\text{--}10^8 \text{ K}$ X-ray gas in radio AGN (including some in our sample), which may bring cold accretion into play. One issue we did not discuss is galaxy merger as many BCGs are dumbbells. Although the connection between the various gas components is unclear, we suggest that the existence of a corona can effectively shield dust and cold gas from strong evaporation and stripping by the ICM, especially in hot clusters.

7.2. Are coronae decoupled from the radio feedback cycle?

If small coronae are responsible to fuel strong radio AGN (either through cold accretion of the cooled materials or through hot accretion), is radio heating responsible to offset strong cooling inside coronae? As a complete radio feedback cycle is generally assumed in large cool cores (summarized in e.g., McNamara & Nulsen 2007), another way to put the question is: is the radio feedback cycle complete in small coronae as in large cool cores? The ICM surrounding a corona is clearly decoupled from the feedback cycle, simply absorbing heat from unrelated radio outbursts. As discussed in S07 and early in this paper, it requires a fine tuning for a strong radio outburst to offset cooling inside a small corona without completely destroying it, which is not a problem for large cool cores. This is more a problem when it is considered that $\sim 20\%$ of BCGs have $L_{1.4\text{GHz}} > 10^{24} \text{ W Hz}^{-1}$ AGN (so the active period of strong heating is a large portion of galaxy's life time, Lin & Mohr 2007) and the ubiquity of small coronae associated with massive galaxies (S07). Other heat sources inside coronae do exist as discussed in S07, e.g., stellar mass loss and SN heating. However, these heating terms should follow the shallow stellar light profile so cooling will always overwhelm within $2\text{--}3 \text{ kpc}$ from the nucleus (S07).

Although strong radio outbursts may simply penetrate small coronae, weak and more frequent radio outbursts are able to release significant amount of heating within the central a few kpc to offset cooling. Nearby examples include M84 (Finoguenov & Jones 2001), NGC 4636 (Jones et al. 2002) and NGC 4552 (Machacek et al. 2006) in the distance of the Virgo cluster. Although their radio AGN are weak ($L_{1.4\text{GHz}} = 0.024 - 1.89 \times 10^{23} \text{ W Hz}^{-1}$), their coronae are significantly disturbed. The radio outbursts in these systems are weak, with energy from $\sim 1.4 \times 10^{55} \text{ ergs}$ to $\sim 6 \times 10^{56} \text{ ergs}$ (Jones et al. 2002; Machacek et al. 2006; Finoguenov et al. 2008), which can be compared with the biggest radio outburst known in clusters, $\sim 1.2 \times 10^{62} \text{ ergs}$ in MS 0735.6+7421 (McNamara et al. 2005, 2009). A $10^{56} - 10^{57} \text{ ergs}$ outburst will not disrupt a luminous

corona too much (e.g., $4 \int PdV \sim 3 \times 10^{57}$ ergs for ESO 137-006's corona), which is about the amount of gentle heating required to offset cooling in a small corona. Thus, gentle heating from weak radio AGN may complete the feedback cycle in coronae. However, this is not exactly the answer to strong radio AGN in the upper portion of the corona class, as it is unknown what will turn them to a lower activity state if the strong radio heating is not involved in the feedback cycle. Maybe radio heating of the coronal gas is only important in weak outbursts, while heating is only on the surrounding ICM in strong outbursts. During the period of strong outbursts, SN heating inside coronae can still offset some cooling and the stellar mass loss can compensate a significant portion of gas cooled out of the hot phase (S07). The detail of energy balance and transfer in these embedded mini-cool cores is beyond the scope of this work. It would also help to know the difference of the radio AGN populations associated with a small corona and associated with a large cool core, e.g., duty cycles. The current large sample studies (e.g., Best et al. 2007; Lin & Mohr et al. 2007) lack enough X-ray data to divide two classes.

A related question is on the origin of the gap in Fig. 1, or the absence of $\sim 10^{42}$ ergs s^{-1} cool cores at $L_{1.4\text{GHz}} > 10^{24}$ W Hz^{-1} . The gap is not observed at low $L_{1.4\text{GHz}}$. Systems that should fill the gap are mainly groups. Why are there so few luminous group cool cores with strong radio AGN? Have that kind of group cool cores been transferred into the corona class in a powerful radio outburst? We estimate the required outburst energy to heat group cool cores beyond ~ 5 kpc radius, from the group pressure profiles derived by S09. Outburst energy of $10^{59} - 10^{60}$ ergs ($4 \int PdV$) is required. The corresponding power in 10^8 yr is $3 \times 10^{43} - 3 \times 10^{44}$ ergs s^{-1} . A radio AGN with $L_{1.4\text{GHz}}$ of $\sim 10^{24}$ W Hz^{-1} can provide that amount of energy on average (Birzan et al. 2008), especially if the biasing factors to the Birzan et al. relation discussed in the last section are considered.

7.3. The implications of the corona class

The existence of a significant number of strong radio AGN in the corona class has important implications for the radio AGN heating and formation of large cool cores. As shown in this work and some previous work (e.g., Hardcastle et al. 2007), ISM accretion in early-type galaxies is sufficient to power FR-I radio AGN, long before a large cluster cool core is formed. The radio outburst injects a large amount of heat into the surrounding ICM and is capable to destroy embryonic large ICM cool cores beyond the central several kpc. Therefore, this provides another way to prevent formation of large cool cores in some clusters, besides the scenario of major mergers at an early stage proposed by Burns et al. (2008). Nevertheless, large cool cores do form. Radio AGN heating in massive clusters may not be strong enough to balance cooling (e.g., Best et al. 2007). A dense corona of a BCG may also not form because of high SN rate and merging rate so the corona feedback has never been triggered to destroy an embryonic ICM cool core. It would be useful to know the percentage of large cool cores (or coronae) for BCGs as a function of the cluster mass. Our heterogeneous sample indeed implies that the fraction of coronae for BCGs increases when the cluster mass decreases (Fig. 1).

The dense coronal gas is also important to maintain the collimation of radio jets (e.g., Fabian & Rees 1995). There is no evidence for slower milli-arcsec scale jets of FR-I sources in comparison to FR-II sources (Giovannini et al. 2001) so the

FR-I jets must slow down from the pc to kpc scale. The existence of a dense corona provides extra pressure to decelerate jets. In the case of ESO 137-006, $\int_0^{r_{\text{cut}}} P_{\text{ISM}} dr / (P_{\text{ICM}} r_{\text{cut}}) = 7.7$.

The best-fit β -model for the density profile was used (Fig. 7) and $r_{\text{cut}} = 4.24$ kpc. This is only a comparison of pressure, without considering the slowing of jets with time. Nevertheless, this simple comparison shows that jet flaring would be at much larger radii if the radio AGN is “naked” in the ICM.

Hardcastle & Sakelliou (2004) studied jet termination in WAT radio sources. They presented an anti-correlation between the jet termination length and the cluster temperature. One scenario listed in the paper is that the jet disruption coincides with the ISM/ICM interface. Seven WATs in their sample are in our sample. Clearly from this work and S07, the ISM coronae have radii of typically a few kpc (also see the pressure argument in S07), at most 9-10 kpc for 3C 465 (S07). The coronae are much smaller than the derived jet termination length (12-74 kpc) by Hardcastle & Sakelliou (2004) so the above scenario can be ruled out. On the other hand, as shown in Sun et al. (2005a; 2005b) and S07, radio jets often turn on after transversing the corona/ICM boundary.

7.4. The B55 and the extended HIFLUGCS samples

Our sample (Table 1) includes nearly all systems in the B55 and the extended HIFLUGCS samples. The B55 sample (55 clusters, Peres et al. 1998) is a hard X-ray selected sample that has been fully covered by *Chandra*. There are no groups ($kT < 2$ keV) in the B55 sample. The basic HIFLUGCS sample has 63 groups and clusters (Reiprich & Böhringer 2002) that has been fully covered by *Chandra*. Reiprich & Böhringer (2002) also listed 11 systems that are brighter than the HIFLUGCS flux limit but within 20 deg from the Galactic plane so that they are not included in the HIFLUGCS sample. We include them and call the resulting sample the extended HIFLUGCS (HIFLUGCS-E) sample. Only the Antlia group does not have *Chandra* data, but its BCG is radio quiet anyway. Instead of marking the B55 and the HIFLUGCS-E systems in Fig. 1, we plot the cooling time at 10 kpc radius of the BCG versus the 1.4 GHz luminosity of the BCG (Fig. 11). The cooling time profiles come from S09, Cavagnolo et al. (2009) and our own work. We choose a radius of 10 kpc to well separate small coronae from large cool cores. Mittal et al. (2009) presented a similar plot for the HIFLUGCS sample, but they used isobaric cooling time at $0.004 r_{500}$ (2 - 6 kpc) and the total radio luminosity. Cavagnolo et al. (2008) presented a plot of the central entropy versus the radio luminosity. Their conclusion of the association between low entropy gas and the strong radio AGN is consistent with ours. In Fig. 11, we did not include A1367 and A754 as they are irregular clusters with the X-ray peak far from their BCGs. In the plot for the HIFLUGCS-E sample, A2163, as the most distant system ($z=0.203$), was excluded.

As shown in Fig. 11, there is a general anti-correlation between the radio activity and the central gas cooling time (e.g., at 10 kpc), especially if groups are excluded. However, there are three outliers in the B55 sample and seven outliers in the HIFLUGCS-E sample. All these BCGs have small coronae. More exactly, the BCGs of A3532 and A3376 are only flagged as soft X-ray sources (or candidates of coronae, see Section 3) as the observations are not deep enough (9.5 - 64 ks with ACIS-I) at their redshifts ($z=0.046-0.055$). As emphasized in Section 3, we are confident that most soft X-ray sources are genuine

thermal coronae. At $L_{1.4\text{GHz}} > 10^{24} \text{ W Hz}^{-1}$, the fraction of coronae increases when the cluster flux limit of the sample decreases, 3 out of 16 in the B55 sample versus 7 out of 21 in the HIFLUGCS-E sample. The fraction is 30 out of 49 (14 out of 33 for $kT > 2 \text{ keV}$ systems) in our sample although ours is not a flux-limit sample. This is not surprising as small flux-limited samples are biased to the local luminous LCC clusters. Owing to its high flux limit, groups in the extended HIFLUGCS sample are luminous groups with large cool cores and none of their BCGs has strong radio activity ($L_{1.4\text{GHz}} > 10^{24} \text{ W Hz}^{-1}$), while these are many such groups in our sample (Fig. 1).

8. CONCLUSIONS

We present a systematic study to search for X-ray cool cores associated with 154 BCGs and 70 strong radio AGN ($L_{1.4\text{GHz}} > 10^{24} \text{ W Hz}^{-1}$) in 145 nearby groups and clusters (178 galaxies in total), selected from the *Chandra* archive, including nearly all systems in the B55 and the extended HIFLUGCS samples. The main conclusions of this work are:

1) All 65 BCGs with strong radio AGN ($L_{1.4\text{GHz}} > 2 \times 10^{23} \text{ W Hz}^{-1}$) have confirmed X-ray cool cores with a central isochoric cooling time of $< 1 \text{ Gyr}$ (Section 4 and Fig. 1). In fact, there are only two non-detections of cool cores out of 77 BCGs above $L_{1.4\text{GHz}}$ of $10^{23} \text{ W Hz}^{-1}$. Upper limits of both non-detections are high so we claim that every BCG with a $L_{1.4\text{GHz}} > 10^{23} \text{ W Hz}^{-1}$ AGN has an X-ray cool core. This conclusion also holds in the B55 and the extended HIFLUGCS samples (Section 7.4). The BCG cool cores can be divided into two classes, large ($r_{4\text{Gyr}} > 30 \text{ kpc}$) and luminous ($L_{0.5-2\text{keV}} \gtrsim 10^{42} \text{ ergs s}^{-1}$) cool cores like Perseus's cool core, or small ($< 4 \text{ kpc}$ in radius typically) coronae like ESO 137-006's in A3627 (Section 5, Fig. 6-7 and S07, also see Fig. 2-3 for more examples). We call them the large-cool-core (LCC) class and the corona class. The gas of the former class is primary of ICM origin, while the latter one is of ISM origin. For 21 non-BCGs with $L_{1.4\text{GHz}} > 10^{24} \text{ W Hz}^{-1}$ AGN, there are only five confirmed corona detections, but most upper limits are high.

2) Small coronae, easily overlooked or misidentified as X-ray AGN at $z > 0.1$, are mini-cool-cores in groups and clusters (Section 4, 5 and 6). They can trigger strong radio outbursts long before large cool cores are formed. The triggered outbursts can destroy embryonic large cool cores and thus provide another mechanism besides mergers to prevent formation of large cool cores (see Burns et al. 2008). The outbursts triggered by coronae can also inject extra entropy into the ICM and modify the ICM properties in systems without large cool cores. For BCGs with strong radio AGN in our sample, the corona fraction is at least comparable to that of large cool cores.

3) There are no groups with a luminous X-ray core ($L_{0.5-2\text{keV}} > 10^{41.8} \text{ ergs s}^{-1}$) hosting a strong radio AGN with $L_{1.4\text{GHz}} > 10^{24} \text{ W Hz}^{-1}$ (Section 4 and Fig. 1). This is not observed in clusters ($kT > 2 \text{ keV}$). The absence of low-mass systems with strong radio AGN creates a gap between the two classes at high radio luminosities (Fig. 1). Although this result needs to be examined with a larger, representative group sample

(e.g., purely optically selected), it may point to a greater impact of feedback on low-mass systems than clusters. We suggest that some groups with a luminous cool core may have been transferred into the corona class in a strong radio outburst.

4) In the LCC class, there is a general trend (albeit with large scatter) that more luminous cool cores host more luminous radio AGN. We suspect that the environmental boosting may play a role to create the trend. BCGs in weak cool cores and noncool cores only have weak radio AGN (Fig. 1, 11 and Section 4).

5) Only $\sim 16\%$ of radio AGN ($L_{1.4\text{GHz}} > 10^{24} \text{ W Hz}^{-1}$) have luminous X-ray AGN ($L_{0.5-10\text{keV}} > 10^{42} \text{ ergs s}^{-1}$), while the X-ray AGN fraction is even smaller for BCGs ($\sim 4\%$). On the other hand, $\gtrsim 80\%$ of strong radio AGN have a confirmed cool core ($\gtrsim 90\%$ for BCGs), which implies their tight connection. For BCGs, all detected X-ray AGN ($L_{0.5-10\text{keV}} > 10^{42} \text{ ergs s}^{-1}$) are also a radio AGN ($L_{1.4\text{GHz}} > 10^{24} \text{ W Hz}^{-1}$, Section 4.3). Thus, a strong X-ray AGN of a BCG only emerges at the stage of its strong radio activity, occasionally.

6) Luminous coronae may be able to power their radio AGN through Bondi accretion (Section 7.1 and Fig. 10, also see Hardcastle et al. 2007), while the hot accretion may not work for faint coronae in less massive galaxies. However, a complete inventory of cold gas in embedded coronae is required to address the question of the accretion mode. We notice that cold ISM and dust indeed exist in some coronae with strong radio AGN.

7) While coronae may trigger radio AGN, strong outbursts have to deposit little energy inside coronae to keep them intact (also emphasized in S07). Thus, it is unclear whether coronae are decoupled from the radio feedback cycle (Section 7.2). On the other hand, weak outbursts can provide gentle heating required to offset cooling in coronae. The existence of coronae around strong radio AGN in groups and clusters also affects the properties of radio jets, e.g., extra pressure to decelerate jets and maintain the collimation of jets.

8) We also present detailed analyses on coronae associated with ESO 137-006 (in A3627) and NGC 4709 (in the Centaurus cluster), as an example of luminous coronae associated with a strong radio AGN (Section 5) and an example of faint coronae (Section 6) respectively.

We are very grateful to Paul Nulsen, Megan Donahue, Christine Jones and Mark Voit for detailed comments and suggestions on an early draft of this paper. We also want to thank Alexey Vikhlinin and Bill Forman for inspiring discussions since the discovery of embedded coronae. We also thank Craig Sarazin, Ken Cavagnolo and Greg Sivakoff for discussions. We thank Ken Cavagnolo for providing his results on some cool-core clusters. We thank Alexey Vikhlinin to provide the proprietary *Chandra* data of A3532 and 3C 88. This research has made use of the NASA/IPAC Extragalactic Database (NED) which is operated by the Jet Propulsion Laboratory, California Institute of Technology, under contract with the National Aeronautics and Space Administration. The financial support for this work was provided by the NASA grant GO7-8081X and the NASA LTSA grant NNG-05GD82G.

REFERENCES

Anders, E., & Grevesse N. 1989, *Geochimica et Cosmochimica Acta*, 53, 197
 Akritas, M. G., & Bershadsky, M. A. 1996, *ApJ*, 470, 706
 Allen, S. et al. 2006, *MNRAS*, 372, 21
 Barthel, P. D., & Arnaud, K. A. 1996, *MNRAS*, 283, L45

Becker, R. H., White, R. L., Helfand, D. J. 1995, *ApJ*, 450, 559
 Begelman, M. C., & Nath, B. 2005, *MNRAS*, 361, 1387
 Best, P. et al. 2005, *MNRAS*, 362, 25
 Best, P. et al. 2006, *MNRAS*, 368, L67

- Best, P. et al. 2007, MNRAS, 379, 894
 Birzan, L. et al. 2008, ApJ, 686, 859
 Bock, D. C.-J., Large, M. I., Sadler, E. M. 1999, AJ, 117, 1578
 Böhringer, H. et al. 1996, ApJ, 467, 168
 Böhringer, H. et al. 2000, ApJS, 129, 435
 Böhringer, H. et al. 2004, A&A, 425, 367
 Burns, J. O. et al. 2008, ApJ, 675, 1125
 Cavagnolo, K. W., Donahue, M., Voit, G. M., Sun, M. 2008, ApJ, 683, L107
 Cavagnolo, K. W., Donahue, M., Voit, G. M., Sun, M. 2009, ApJS, in press, arXiv:0902.1802
 Chen, Y., Reiprich, T. H., Böhringer, H., Ikebe, Y., Zhang, Y.-Y. 2007, A&A, 466, 805
 Churazov, E. et al. 1999, ApJ, 520, 105
 Churazov, E. et al. 2005, MNRAS, 363, L91
 Condon, J. J. et al. 1998, AJ, 115, 1693
 Croston, J. H. et al. 2008, MNRAS, 386, 1709
 Croton, D. J. et al. 2006, MNRAS, 365, 11
 de Koff, S. et al. 2000, ApJS, 129, 33
 Evans, A. S. et al. 2005, ApJS, 159, 197
 Evans, D. A. et al. 2006, ApJ, 642, 96
 Faber, S. & Gallagher, J. 1976, ApJ, 204, 365
 Fabian, A. C., & Rees, M. J. 1995, MNRAS, 277, L55
 Finoguenov, A., & Jones, C. 2001, ApJ, 547, L107
 Finoguenov, A. et al. 2008, ApJ, 686, 911
 Gastaldello, F., Buote, D. A., Brighenti, F., Mathews, W. G. 2008, ApJ, 673, L17
 Giovannini, G., Cotton, W. D., Feretti, L., Lara, L., Venturi, T. 2001, ApJ, 552, 508
 Hardcastle, M. J., Birkinshaw, M., Worrall, D. M. 2001, MNRAS, 326, 1499
 Hardcastle, M. J. et al. 2002, MNRAS, 334, 182
 Hardcastle, M. J. et al. 2005, MNRAS, 358, 843
 Hardcastle, M. J., & Sakelliou, I. 2004, MNRAS, 349, 560
 Hardcastle, M. J. et al. 2007, MNRAS, 376, 1849
 Iwamoto, K. et al. 1999, ApJS, 125, 439
 Jeltema, T. E., Binder, B., Mulchaey, J. S. 2008, ApJ, 679, 1162
 Jones, P. A., & McAdam, W. B. 1996, MNRAS, 282, 137
 Jones, C. et al. 2002, ApJ, 567, L115
 Kauffmann, G. et al. 2004, MNRAS, 353, 713
 Kim, D. W., & Fabbiano, G. 2004, ApJ, 611, 846
 Kraft, R. P. et al. 2006, ApJ, 639, 753
 Li, Jingqiang et al. 2004, ApJ, 610, 1204
 Lim, J. et al. 2000, ApJ, 545, L93
 Lim, J. et al. 2003, ASP Conf. Series 290, 529
 Lin, Y. T., & Mohr, J. J. 2007, ApJS, 170, 71
 Machacek, M., Nulsen, P. E. J., Jones, C., Forman, W. R. 2006, ApJ, 648, 947
 Marconi, A., & Hunt, L. K. 2003, ApJ, 589, L21
 Mathews, W. G. & Brighenti, F. 2003, ApJ, 590, L5
 McNamara, B. R. et al. 2005, Nature, 433, 45
 McNamara, B. R., & Nulsen, P. E. J. 2007, ARA&A, 45, 117
 McNamara, B. R. et al. 2009, ApJ, in press, arXiv:0811.3020
 Mittal, R. et al. 2009, A&A, in press, arXiv:0810.0797
 Parma, P., Murgia, M., de Ruiter, H. R., Fanti, R., Mack, K.-H., Govoni, F. 2007, A&A, 470, 875
 Peres, C. B. et al. 1998, MNRAS, 298, 416
 Prandoni, I. et al. 2007, NewAR, 51, 43
 Pratt, G. W., Croston, J. H., Arnaud, M., Böhringer, H. 2009, A&A, in press, arXiv:0809.3784
 Proga, D., & Begelman, M. C. 2003, ApJ, 592, 767
 Rafferty, D. A. et al. 2008, ApJ, 687, 899
 Reiprich, T. H., Böhringer, H. 2002, ApJ, 567, 716
 Revnivtsev, M., Churazov, E., Sazonov, S., Forman, W., Jones, C. 2008, A&A, 490, 37
 Sadler, E. M. et al. 2002, MNRAS, 329, 227
 Scannapieco, E. et al. 2005, ApJ, 635, L13
 Shabala, S. S., Ash, S., Alexander, P., Riley, J. M. 2008, MNRAS, 388, 625
 Shibata, R. et al. 2001, ApJ, 549, 228
 Simões Lopes, R. D. et al. 2007, ApJ, 655, 718
 Sun, M., Vikhlinin, A., Forman, W., Jones, C., Murray, S. S. 2005a, ApJ, 619, 169
 Sun, M., Jerius, D., Jones, C. 2005b, ApJ, 633, 165
 Sun, M. et al. 2007, ApJ, 657, 197 (S07)
 Sun, M. et al. 2009, ApJ, 693, 1142 (S09)
 Tonry, J. L. et al. 2001, ApJ, 546, 681
 Tremblay, G. R. et al. 2006, ApJ, 643, 101
 van Dokkum, P. G., & Franx, M. 1995, AJ, 110, 2027
 Verdoes Kleijn, G. A., & de Zeeuw, P. T. 2005, A&A, 435, 43
 Vikhlinin, A., Markevitch, M., Forman, W., Jones, C. 2001, ApJ, 555, L87
 Voit, G. M. 2005, Rev. of Mod. Physics, 77, 207
 von der Linden, A. et al. 2007, MNRAS, 379, 867
 Worrall, D. M., Birkinshaw, M., Hardcastle, M. J. 2003, MNRAS, 343, L73
 Wilson, A. S., & Colbert, E. J. M. 1995, ApJ, 438, 62
 Woudt, P. A., & Kraan-Korteweg, R. C. 2001, A&A, 380, 441
 Yamasaki, N. Y., Ohashi, T., Furusho, T. 2002, ApJ, 578, 833

TABLE 1
THE SAMPLE OF 145 GROUPS AND CLUSTERS

System	z^a	N ^b	System	z^a	N ^b	System	z^a	N ^b	System	z^a	N ^b	System	z^a	N ^b
Centaurus	0.0114	8	A3581	0.0230	1	A1142	0.0349	1	A193	0.0486	1	A695	0.0687	2
NGC 1550	0.0124	4	NGC 5129	0.0230	2	A2063	0.0349	4	A3562	0.0490	1	A514	0.0713	1
NGC 7619	0.0125	2	Coma	0.0231	9	2A0335+096	0.0349	3	SC1327-312	0.0495	1	A744	0.0729	1
IC 4296	0.0125	2	NGC 1132	0.0233	1	A2147	0.0350	1	A2717	0.0498	2	A2462	0.0733	1
A1060	0.0126	1	A400	0.0244	1	A2052	0.0355	2	A3395S	0.0506	1	A3112	0.0752	5
NGC 6482	0.0131	1	UGC 2755	0.0245	1	ESO 306-017	0.0358	2	A1377	0.0514	1	A2670	0.0761	1
Pavo	0.0137	1	3C296	0.0247	1	A2151	0.0366	1	A3391	0.0514	1	A2029	0.0773	3
HCG62	0.0137	1	NGC 6251	0.0247	2	NGC 5098	0.0368	2	A3528S	0.0530	1	RXJ 1159+5531	0.0808	1
NGC 5419	0.0138	2	NGC 4325	0.0257	1	A576	0.0389	1	Hydra A	0.0539	4	A1650	0.0839	8
NGC 4782	0.0144	1	3C 442A	0.0263	4	RBS540	0.0390	1	A754	0.0542	7	A2597	0.0852	3
NGC 2563	0.0149	6	MKW8	0.0270	1	A3571	0.0391	1	RXJ 1022+3830	0.0543	1	A478	0.0881	11
NGC 3402	0.0153	1	UGC 5088	0.0274	1	AS463	0.0394	2	A85	0.0551	9	A2142	0.0909	4
NGC 1600	0.0156	2	NGC 6338	0.0274	1	A1139	0.0398	1	A2626	0.0553	1	3C388	0.0917	2
A3627	0.0162	5	NGC 4104	0.0282	1	A2657	0.0402	1	A3532	0.0554	1	A2384	0.0943	1
A262	0.0163	2	A539	0.0284	2	A2572	0.0403	1	A3667	0.0556	9	A2244	0.0968	1
NGC 507	0.0164	2	Ophiuchus	0.0291	1	A2107	0.0411	1	A2319	0.0557	1	PKS 0745-191	0.103	3
NGC 315	0.0165	1	RBS 461	0.0296	1	A2589	0.0414	4	Cygnus A	0.0561	11	A1446	0.104	1
NGC 777	0.0167	1	A4038	0.0300	2	NGC 2484	0.0428	1	AS1101	0.0564	1	RX J1852.1+5711	0.109	1
3C 31	0.0170	1	A2199	0.0302	2	A119	0.0442	2	A133	0.0566	3	A562	0.110	1
3C 449	0.0171	1	3C88	0.0302	1	A160	0.0447	1	ESO 351-021	0.0571	1	A2220	0.110	1
AWM7	0.0172	1	ZW1615+35	0.0310	4	A168	0.0450	2	A2256	0.0581	3	HCG 51	0.0258	2
NGC 7618	0.0173	3	ESO 552-020	0.0314	1	MKW3S	0.0450	1	A3880	0.0581	1			
Perseus	0.0179	19	A2634	0.0314	1	UGC 842	0.0452	1	A1991	0.0587	1			
A194	0.0180	2	A1177	0.0316	1	A3376	0.0456	2	A3266	0.0589	2			
NGC 533	0.0185	1	A1185	0.0325	1	A1736	0.0458	1	A3158	0.0597	3			
NGC 741	0.0185	1	IC 1262	0.0326	4	A1644	0.0473	2	A3128	0.0599	1			
MKW4	0.0200	1	A496	0.0329	3	NGC 326	0.0474	1	A3125	0.0611	2			
3C129.1	0.0210	2	A1314	0.0335	1	A4059	0.0475	2	AS405	0.0613	1			
3C66B	0.0212	1	IC1880	0.0340	1	A3556	0.0479	1	A1795	0.0625	13			
A1367	0.0220	3	UGC3957	0.0341	1	A3558	0.0480	1	A2734	0.0625	1			
NGC 5171	0.0229	1	NGC 6269	0.0348	1	SC1329-313	0.0482	1	A1275	0.0637	1			

^aThe redshift is from NASA/IPAC Extragalactic Database (NED)

^bThe number of *Chandra* observations

TABLE 2
GALAXIES IN THE CORONA CLASS WITH $L_{1.4\text{GHz}} > 10^{24} \text{ W Hz}^{-1}$ AGN

Galaxy (Cluster)	$L_{K_s}^a$	$L_{1.4\text{GHz}}^b$	$L_{0.5-2\text{keV}}^c$	kT (keV)	Note ^d
IC 4296 (IC 4296)	11.82	24.14	1.50 ± 0.12	0.68 ± 0.02	BCG, $2.9 \times 10^{41} \text{ erg s}^{-1}$ AGN
3C 278 (NGC 4782)	11.81	24.54	0.223 ± 0.016	0.72 ± 0.03	BCG
ESO 137-006 (A3627)	11.77	25.39	1.69 ± 0.08	0.91 ± 0.02	BCG
ESO 137-007 (A3627)	11.44	24.39	< 0.13		NAT, X-ray PS
NGC 315 (NGC 315)	11.88	24.12	1.97 ± 0.06	0.59 ± 0.01	BCG, $8.0 \times 10^{41} \text{ erg s}^{-1}$ AGN
3C 31 (3C 31)	11.70	24.49	0.667 ± 0.027	0.71 ± 0.02	BCG, $1.0 \times 10^{41} \text{ erg s}^{-1}$ AGN
3C 449 (3C 449)	11.16	24.38	0.201 ± 0.026	$0.62^{+0.15}_{-0.07}$	BCG
NGC 1265 (Perseus)	11.60	24.79	0.322 ± 0.039	0.63 ± 0.03	NAT
NGC 547 (A194)	11.74	24.45	0.810 ± 0.020	0.66 ± 0.01	BCG
3C 129.1 (3C129.1)	11.66	24.28	0.91 ± 0.26	$0.93^{+0.32}_{-0.60}$	BCG
3C 129 (3C129.1)	11.50	24.75	< 0.22		NAT, X-ray PS
3C 66B (3C 66B)	11.58	24.91	0.656 ± 0.040	0.59 ± 0.03	BCG, $3.0 \times 10^{41} \text{ erg s}^{-1}$ AGN
NGC 3862 (A1367)	11.52	24.77	$0.14^{+0.09}_{-0.05}$	$0.65^{+0.29}_{-0.09}$	BCG
3C 75 (A400)	12.06	24.90	0.973 ± 0.076	$0.71 \pm 0.08, 0.76 \pm 0.08$	BCG, two coronae added
UGC 2755 (UGC 2755)	11.51	24.28	0.904 ± 0.108	0.62 ± 0.06	BCG, $1.7 \times 10^{41} \text{ erg s}^{-1}$ AGN
3C 296 (3C 296)	11.91	24.78	1.3 ± 0.1	0.72 ± 0.02	BCG, $3.2 \times 10^{41} \text{ erg s}^{-1}$ AGN
NGC 6251 (NGC 6251)	11.81	24.55	1.25 ± 0.12	0.70 ± 0.03	BCG, $8.5 \times 10^{42} \text{ erg s}^{-1}$ AGN
3C 442A (3C 442A)	11.78	24.73	3.21 ± 0.20	0.96 ± 0.03	BCG (two galaxies added), $r \sim 25 \text{ kpc}$ core
3C 88 (3C 88)	11.40	25.03	2.75 ± 0.30	0.73 ± 0.06	BCG, $r \sim 25 \text{ kpc}$ core, $\sim 8 \times 10^{41} \text{ erg s}^{-1}$ AGN
NGC 6109 (ZW 1615+35)	11.49	24.64	0.754 ± 0.102	0.58 ± 0.05	NAT
3C 465 (A2634)	11.91	25.21	2.18 ± 0.35	1.01 ± 0.03	BCG
GIN 190 (A496)	11.27	24.26	< 0.12		NAT, X-ray PS
2MASX J03381409+1005038 (2A0335+096)	11.71	24.06	< 0.23		NAT, $7.6 \times 10^{41} \text{ erg s}^{-1}$ AGN
PKS 0427-53 (A5463)	11.92	25.32	0.791 ± 0.070	$0.89^{+0.10}_{-0.15}$	BCG
NGC 2484 (NGC 2484)	11.96	25.05	1.61 ± 0.42	$0.72^{+0.11}_{-0.16}$	BCG, $1.6 \times 10^{42} \text{ erg s}^{-1}$ AGN
UGC 583 (A119)	11.76	24.79	0.770 ± 0.092	0.69 ± 0.06	NAT
CGCG 384-032 (A119)	11.50	24.72	< 0.21		NAT, weak PS
GIN 049 (A160)	11.71	24.68	0.418 ± 0.065	$1.10^{+0.14}_{-0.10}$	BCG
PMN J1326-2707 (A1736)	11.52	24.08	< 0.34		weak PS
PGC 018297 (A3376)	11.52	24.28	0.32 ± 0.13	$0.60^{+0.16}_{-0.15}$	BCG, code 3
NGC 326 (NGC 326)	11.96	24.98	0.740 ± 0.056	0.65 ± 0.04	BCG
PKS 0625-545 (A3395S)	11.76	25.31	1.35 ± 0.28	$1.45^{+0.20}_{-0.13}$	BCG
PKS 0625-53 (A3391)	12.07	25.60	1.05 ± 0.20	0.90 ± 0.13	BCG
PGC 025672 (A754)	11.57	24.63	< 3.6		NAT, $1.4 \times 10^{43} \text{ erg s}^{-1}$ AGN
PGC 025790 (A754)	11.63	24.41	< 0.90		NAT, $3.3 \times 10^{41} \text{ erg s}^{-1}$ AGN
2MASX J09101737-0937068 (A754)	11.74	24.49	0.97 ± 0.30	$0.95^{+0.22}_{-0.19}$	NAT, code 3
PKS 1254-30 (A3532)	12.02	24.91	0.84 ± 0.30	$1.00^{+0.36}_{-0.42}$	BCG, code 3
PGC 064228 (A3667)	11.32	24.60	< 0.30		NAT, $5.2 \times 10^{42} \text{ erg s}^{-1}$ AGN
PKS 0326-536 (A3125)	11.43	24.50	< 0.39		NAT, weak PS
2MASX J03275206-5326099 (A3125)	11.52	24.29	< 0.60		NAT, weak PS
2MASX J22275066-3033431 (A3880)	11.25	24.25	< 2.0		NAT, $1.1 \times 10^{43} \text{ erg s}^{-1}$ AGN
PKS 0429-61 (A3266)	10.70	25.14	< 0.14		NAT, no X-ray
4C +32.26 (A695)	11.76	24.92	0.683 ± 0.120	0.97 ± 0.11	BCG, $r \sim 20 \text{ kpc}$ core, $3.0 \times 10^{41} \text{ erg s}^{-1}$ AGN
2MASX J04483058-2030478 (A514)	11.63	24.93	0.73 ± 0.19	$0.93^{+0.18}_{-0.14}$	NAT, code 3
2MASX J04481046-2024574 (A514)	11.48	24.24	< 1.5		NAT, $1.1 \times 10^{42} \text{ erg s}^{-1}$ AGN
2MASX J04480299-2026384 (A514)	11.32	24.16	< 0.47		NAT, $1.2 \times 10^{41} \text{ erg s}^{-1}$ AGN
PKS 2236-17 (A2462)	11.85	25.38	1.40 ± 0.10	0.81 ± 0.05	BCG
B2 1556+27 (A2142)	11.36	24.37	< 0.60		NAT, $2.1 \times 10^{42} \text{ erg s}^{-1}$ AGN
4C +58.23 (A1446)	11.94	25.36	1.09 ± 0.22	$1.00^{+0.27}_{-0.16}$	BCG
4C +69.08 (A562)	11.94	25.62	1.35 ± 0.27	0.75 ± 0.10	BCG
SBS 1638+538 (A2220)	12.26	25.31	1.64 ± 0.33	$0.96^{+0.12}_{-0.28}$	BCG, code 3

^a2MASS K_s band luminosity of the galaxy as shown as $\log(L_{K_s}/L_{\odot})$, $M_{K_{\odot}} = 3.39 \text{ mag}$.

^b1.4 GHz luminosity of the galaxy as shown as $\log(L_{1.4\text{GHz}}/\text{W Hz}^{-1})$ from the NRAO VLA Sky Survey (NVSS) or the Sydney University Molonglo Sky Survey (SUMSS), assuming a spectral index of -0.8.

^cThe rest-frame 0.5 - 2 keV luminosity in unit of $10^{41} \text{ ergs s}^{-1}$

^dBCGs are marked. Most of non-BCGs are NAT sources. The AGN luminosity (measured in the rest-frame 0.5 - 10 keV) is listed if it is higher than $10^{41} \text{ ergs s}^{-1}$. "code 3" refers to "soft X-ray sources" defined in S07 and Section 3.

TABLE 3
FRACTIONS OF X-RAY AGN AND COOL CORES

Sample	Fraction of $L_{0.5-10\text{keV}} > 10^{42} \text{ ergs s}^{-1}$ AGN	Fraction of X-ray cool cores ^a
BCGs with $L_{1.4\text{GHz}} > 10^{24} \text{ W Hz}^{-1}$	6/49	49/49
BCGs with $L_{1.4\text{GHz}} > 10^{23} \text{ W Hz}^{-1}$	6/77	> 75/77
All $L_{1.4\text{GHz}} > 10^{24} \text{ W Hz}^{-1}$ galaxies	11/70	> 54/70
All BCGs	6/154	> 138/154

^aThe fractions of coronae are $\sim 60\%$ in the first sample and $\gtrsim 50\%$ in the other three (Section 4).

TABLE 4
THE CORONAE OF ESO 137-006 AND NGC 4709

Property ^a	ESO 137-006	NGC 4709
Cluster (z)	A3627 (0.0162)	Centaurus (0.0114)
$\log(L_{\text{Ks}}/L_{\odot})$	11.77	11.27
$\log(L_{1.4\text{GHz}}/\text{W Hz}^{-1})$	25.39	<20.88
r_{cut} (kpc)	4.24 ± 0.20	~ 2.0
kT (keV)	0.91 ± 0.02^b	0.78 ± 0.09
O (solar)	$0.52^{+0.63}_{-0.40}$	(0.8)
Ne (solar)	$4.14^{+2.38}_{-1.51}$	(0.8)
Mg (solar)	$2.27^{+1.19}_{-0.70}$	(0.8)
Si (solar)	$1.66^{+0.82}_{-0.48}$	(0.8)
S (solar)	$2.76^{+1.55}_{-0.99}$	(0.8)
Fe (Ni) (solar)	$1.13^{+0.49}_{-0.28}$	(0.8)
$f_{0.5-2\text{keV,thermal,obs}}$ (ergs cm ⁻² s ⁻¹)	$(1.77 \pm 0.09) \times 10^{-13}$	$(9.5 \pm 1.8) \times 10^{-15}$
$L_{0.5-2\text{keV,thermal}}$ (ergs s ⁻¹)	$(1.69 \pm 0.08) \times 10^{41}$	$(1.89 \pm 0.36) \times 10^{39}$
$L_{\text{bol,thermal}}$ (ergs s ⁻¹)	$(2.76 \pm 0.14) \times 10^{41}$	$(3.1 \pm 0.6) \times 10^{39}$
$L_{0.3-8\text{keV,LMXB}} (r < r_{\text{cut}})$ (ergs s ⁻¹)	$(5.2 \pm 1.1) \times 10^{40}$	$\sim 5.3 \times 10^{39}$
$L_{0.3-8\text{keV,LMXB}} (r = r_{\text{cut}} - 11.1 \text{ kpc})$ (ergs s ⁻¹)	$(4.1 \pm 0.8) \times 10^{40}$	-
$L_{0.3-10\text{keV,nucleus}}$ (ergs s ⁻¹)	$< 4 \times 10^{39}$	$< 5 \times 10^{38}$
$n_{\text{e,center}}$ (cm ⁻³)	~ 0.5	~ 0.034
$t_{\text{cooling,center}}$ (Myr)	~ 7	~ 130
M_{gas} (M _⊙)	$(1.78 \pm 0.15) \times 10^8$	$\sim 2.9 \times 10^6$

^aThe energy bands are all measured in the rest-frame.

^bSee Fig. 7 for ESO 137-006's temperature profile.

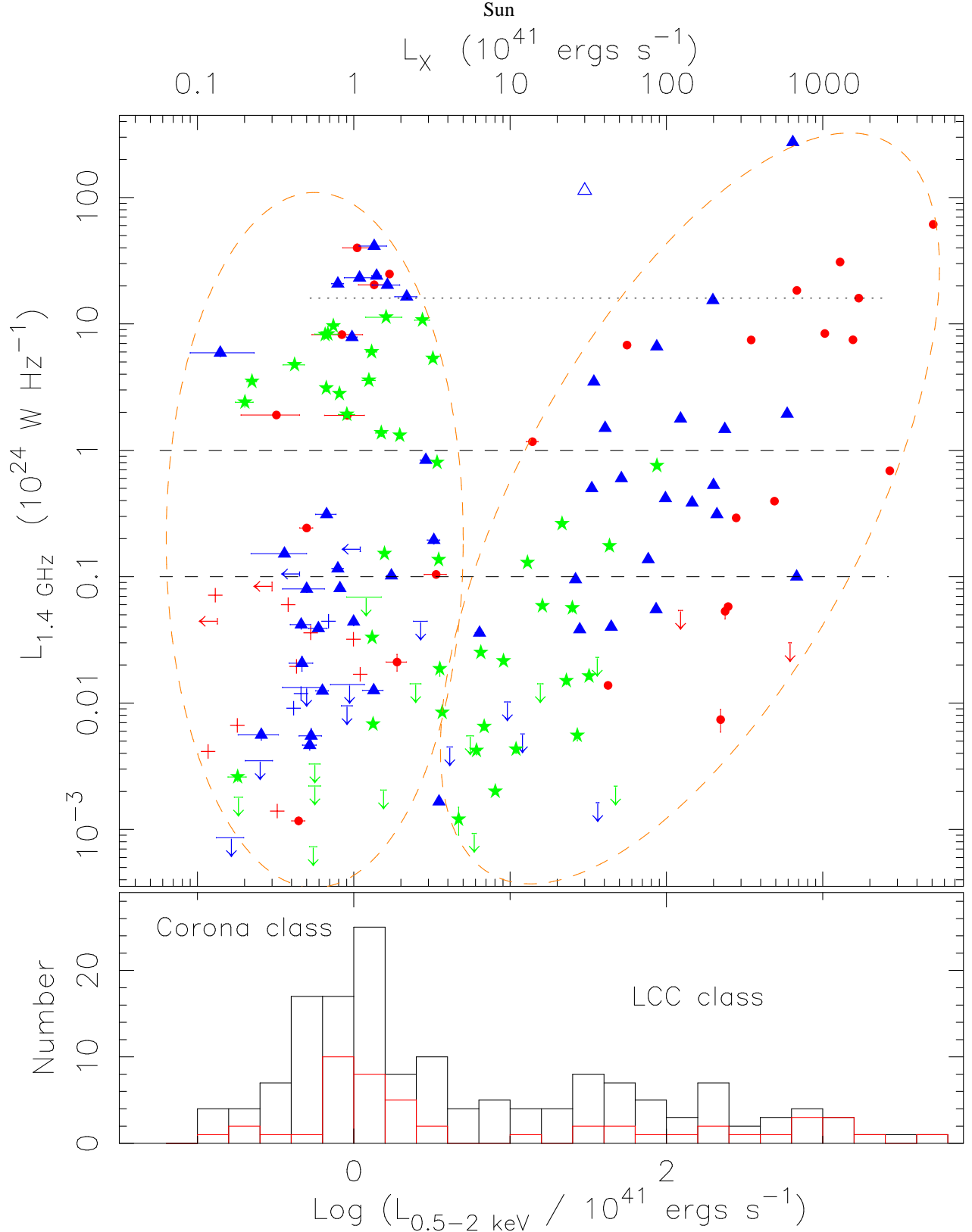


FIG. 1.— The upper panel shows the rest-frame 0.5-2 keV luminosity of the cool core (within a radius where the cooling time is 4 Gyr) of the BCG vs. the 1.4 GHz luminosity of the BCG. Red filled circles are for $kT > 4 \text{ keV}$ clusters. Blue triangles are for $kT = 2-4 \text{ keV}$ poor clusters. Green stars are for $kT < 2 \text{ keV}$ groups. Crosses represent upper limits in both axes. The horizontal dashed lines are $L_{1.4 \text{ GHz}} = 10^{24}$ and $10^{23} \text{ W Hz}^{-1}$. The horizontal dotted line marks $L_{1.4 \text{ GHz}}$ of Perseus's BCG. The lower panel shows the histogram for all BCGs (upper limits included) with two classes marked, while the histogram in red is for $L_{1.4 \text{ GHz}} > 10^{24} \text{ W Hz}^{-1}$ BCGs. At least three interesting results are revealed in this plot. First, there are two classes of BCG cool cores (shown in orange ellipses): the large-cool-core (LCC) class and the corona class. Their dividing line is $\sim 4 \times 10^{41} \text{ ergs s}^{-1}$. Above $L_{1.4 \text{ GHz}} > 10^{23} \text{ W Hz}^{-1}$, every BCG has a confirmed cool core, either in the LCC class or in the corona class, except for two BCGs with high upper limits. In this work, most $L_{1.4 \text{ GHz}} > 10^{24} \text{ W Hz}^{-1}$ BCGs (30 out of 49) are in the corona class. Second, there is a general trend (with large scatter) in the LCC class. More luminous cool cores generally host more luminous radio AGN, or the LCC class is tilted. The slope from the BCES Orthogonal fit is 1.91 ± 0.20 . Third, there are no groups with a luminous cool core ($> 6 \times 10^{41} \text{ ergs s}^{-1}$) that host a radio AGN more luminous than $10^{24} \text{ W Hz}^{-1}$. This is not observed in clusters with strong radio AGN in low-mass systems also causes a gap between the two classes at high radio luminosities. Cygnus A is excluded in this plot as its position ($7.7 \times 10^{43} \text{ ergs s}^{-1}$, $1.2 \times 10^{28} \text{ W Hz}^{-1}$) is so far away from those of others. The only other source that is far from the two ellipses is 3C 388 (the open blue triangle between two classes), which is also a FR-II galaxy like Cygnus A (Kraft et al. 2006).

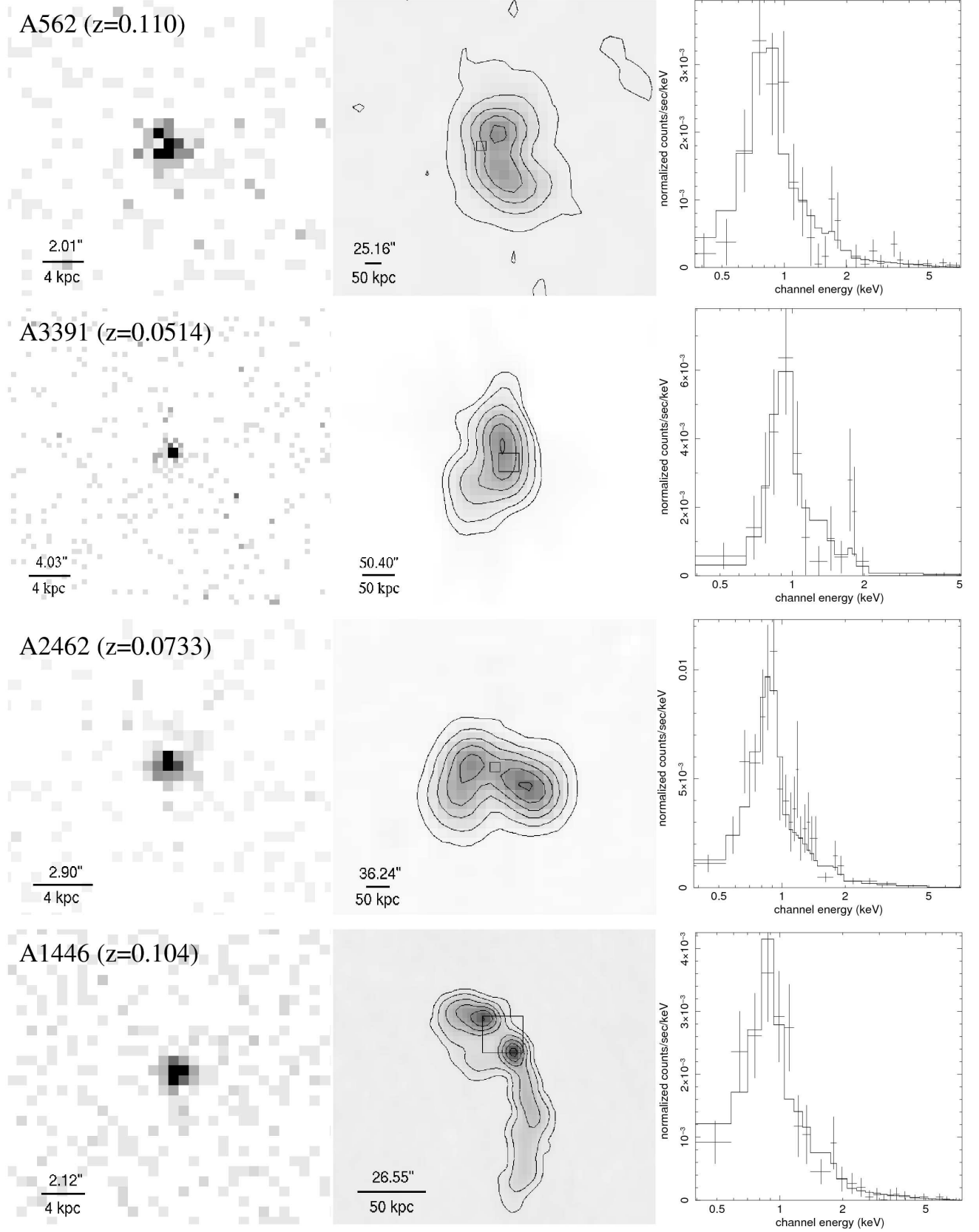


FIG. 2.— Four of the five most luminous radio AGN in the corona class (the 3rd most luminous one, ESO 137-006, is discussed in Section 5 and shown in Fig. 6): the BCGs of A562, A3391, A2462 and A1446. The left panel shows the $0.5 - 3$ keV *Chandra* unbinned image. Coronae are usually hardly resolved at their redshifts. The middle panel shows the radio image and contours from NVSS, FIRST or SUMSS. The small box shows the region of the left panel. These radio sources have luminosities of 1.4 - 2.6 times Perseus's ($L_{1.4\text{GHz}} = 1.6 \times 10^{25} \text{ W Hz}^{-1}$, shown as a dotted line in Fig. 1). The right panel shows the spectrum of the corona. The iron L-shell hump is significant in all cases, unambiguously confirming the existence of thermal gas.

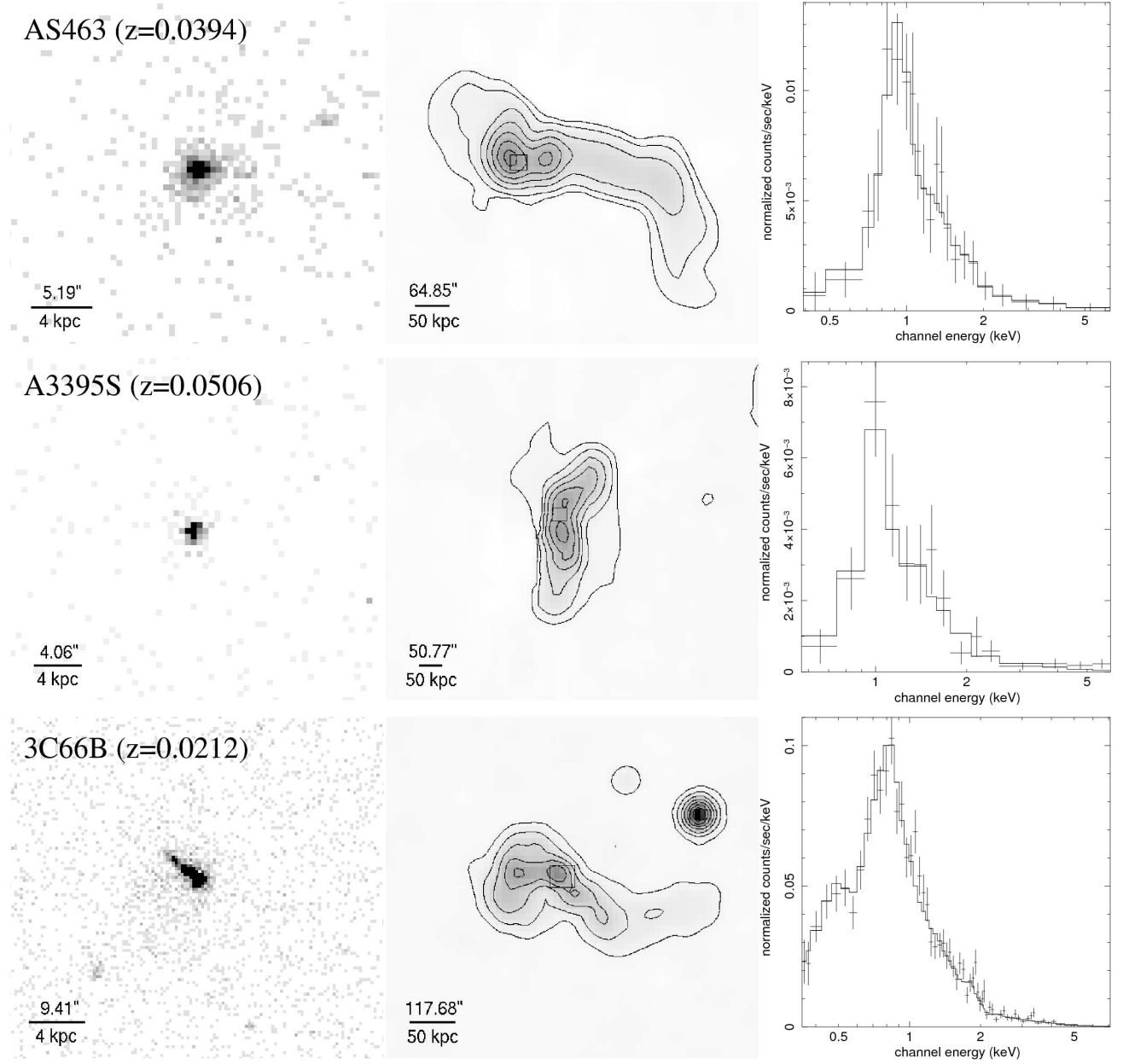


FIG. 3.— Similar to Fig. 2, but for BCGs in AS463 and A3395S, the sixth and seventh most luminous radio AGN (both are 1.3 times Perseus's) in the corona class. AS463's corona is clearly resolved owing to its relative proximity and sufficient *Chandra* exposure (58 ks). We also show an example of a small corona associated with a group's BCG, 3C 66B with a radio AGN that has half the luminosity of Perseus's. Despite its bright nuclear source and X-ray jet, a corona is clearly resolved and the iron L-shell hump is significant (also see Hardcastle et al. 2001; Croston et al. 2003).

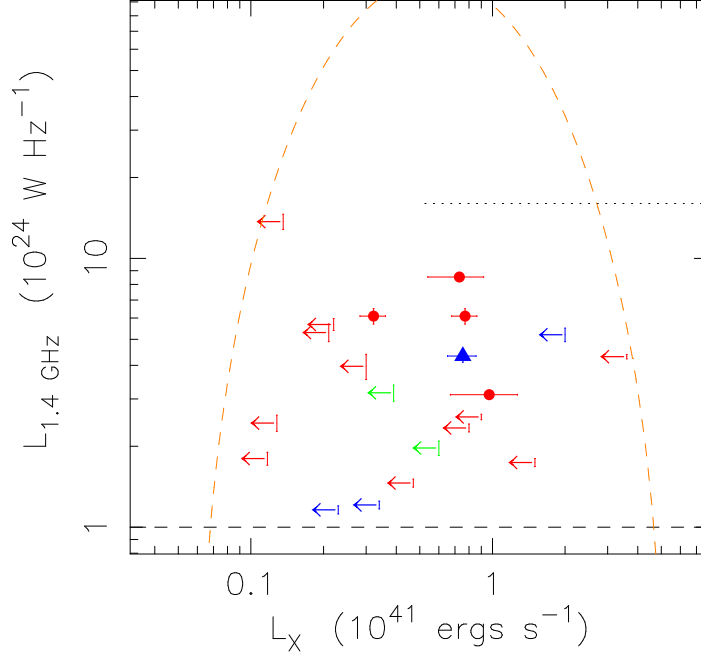


FIG. 4.— The same plot as Fig. 1 but for non-BCGs with $L_{1.4\text{GHz}} > 10^{24} \text{ W Hz}^{-1}$ (the dashed line). The same orange ellipse for the corona class and the dotted line as Fig. 1 are shown. Above the $L_{1.4\text{GHz, cut}}$, BCGs outnumber non-BCGs, 49 vs. 21, because of the limited FOV of *Chandra* (often centered on BCGs) and the enhanced radio AGN activity of BCGs. Most non-BCGs do not have confirmed coronae but most upper limits are high (see Fig. 5).

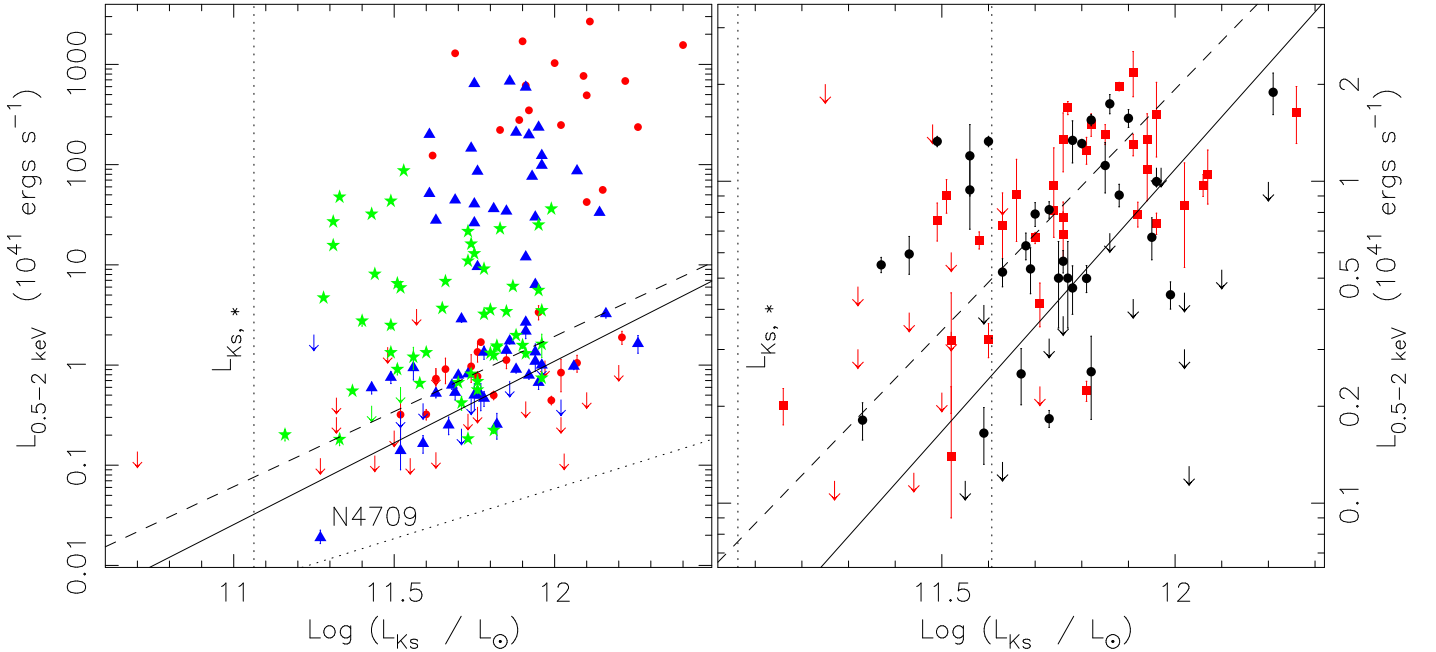


FIG. 5.— **Left:** 0.5-2 keV luminosity of the cool core (within a radius where the cooling time is 4 Gyr) of the galaxy (including both BCGs and non-BCGs) vs. the 2MASS K_s luminosity of the galaxy. Red points are for $kT > 4$ keV clusters. Blue triangles are for $kT = 2-4$ keV poor clusters. Green stars are for $kT < 2$ keV groups. For coronae, the LMXB + nuclear emission has been subtracted as a power-law component is always included in spectral fits. The solid line is the best fit for both detections and upper limits of coronae in rich clusters from S07, while the dashed line is the best fit for only detections from S07. Large cool cores that are mostly composed of ICM form a different population with higher X-ray luminosities than coronae that are composed of ISM. $L_{Ks,*}$ is marked by the vertical dotted line. The position of NGC 4709 is marked, which is the faintest corona known for galaxies more luminous than $L_{Ks,*}$ (see Section 6). The dotted line is the expected emission from cataclysmic variables and coronally active stars (Revnivtsev et al. 2008). As discussed in Section 6, the real contribution is even much smaller as we always used the immediate local background that also includes much stellar emission. **Right:** The same plot as the left one, but only for sources with $L_{0.5-2\text{keV}} < 2.5 \times 10^{41} \text{ ergs s}^{-1}$ (excluding small cool cores). The red squares and upper limits are for $L_{1.4\text{GHz}} > 10^{24} \text{ W Hz}^{-1}$ galaxies, while the black points and upper limits are for $L_{1.4\text{GHz}} < 10^{24} \text{ W Hz}^{-1}$ galaxies. At $L_{Ks} > 3.5L_{Ks,*}$ (the dotted line), radio luminous AGN are generally more luminous in X-rays than radio faint AGN (medians: $\sim 9.5 \times 10^{40} \text{ ergs s}^{-1}$ vs. $\sim 5.5 \times 10^{40} \text{ ergs s}^{-1}$).

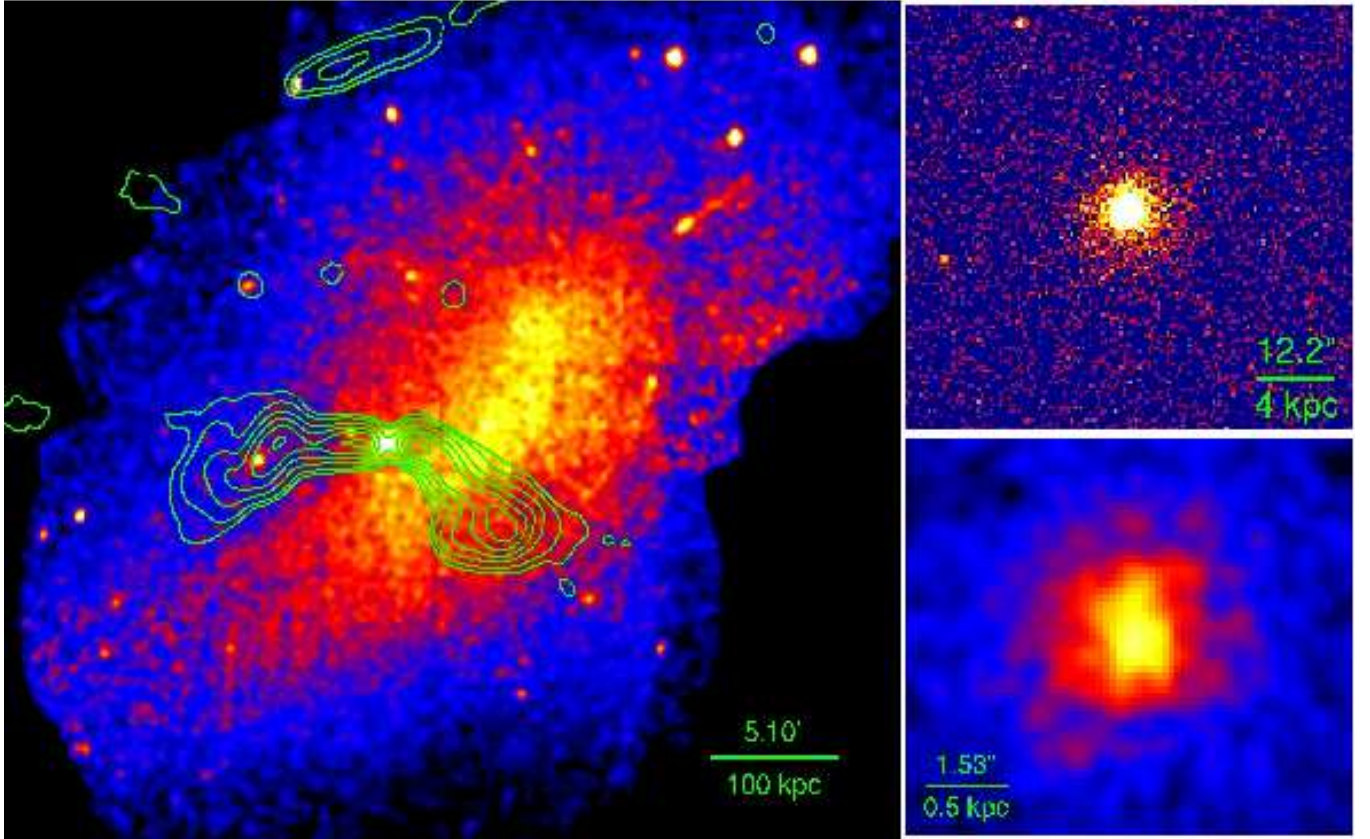


FIG. 6.— 843 MHz contours of ESO 137-006 (from SUMSS, in green) overlaid on the 0.5 - 2 keV XMM-Newton mosaic image of A3627. Evidence indicative of interactions between radio plasma and the ICM is present, including the positional coincidence of the southern boundary of the eastern lobe with the eastern sharp edge of the ICM core and the expanding of the western radio lobe beyond the bright ICM core. The small right panel at the top shows the 0.5 - 5 keV *Chandra* image centered on ESO 137-006. The nearby point sources show the size of the local PSF. ESO 137-006's corona is more extended to the south, which implies its motion to the north and is consistent with the bending of the radio lobes. The small panel at the bottom shows the central region of the corona, after applying the ACIS Subpixel Event Repositioning tool (Li et al. 2004). The core is elongated in the north-south, which is perpendicular to the jet directions.

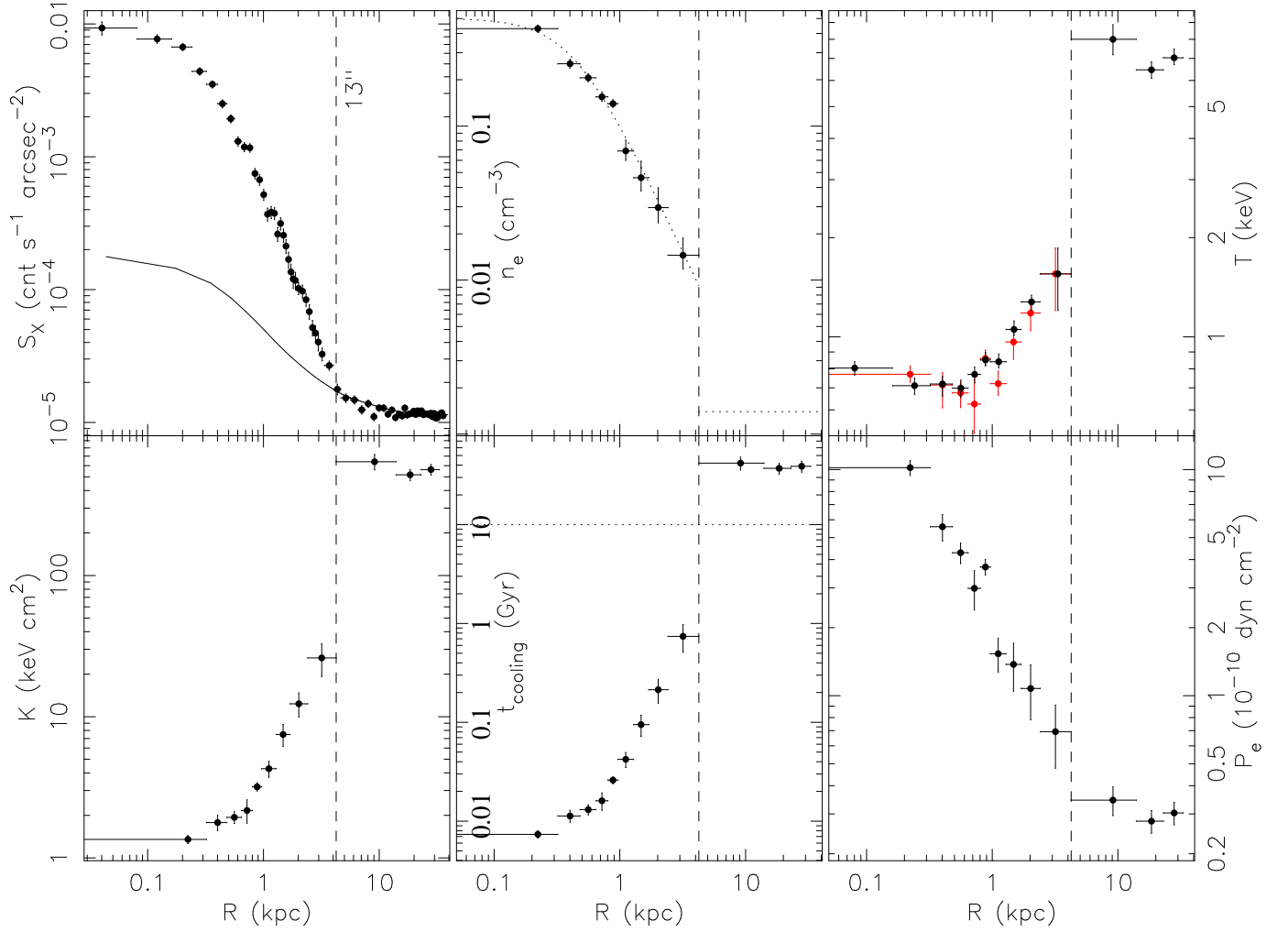


FIG. 7.— Properties of ESO 137-006's corona and its surroundings are shown. The *upper panel* shows the 0.5 - 2 keV surface brightness profile, the electron density profile and the temperature profile. The solid line in the left plot is the predicted LMXB light + the local background, which well describes the surface brightness profile beyond r_{cut} (the vertical dashed line, $13''$). The dotted line in the middle plot is the best-fit β -model of the density profile, while the horizontal dotted line is the average surrounding ICM density. The red data points in the right are the deprojected temperature values. The *lower panel* shows the entropy, cooling time and pressure profiles. The whole corona region has low entropy and short cooling time (< 1 Gyr). Extrapolating the coronal gas pressure to the edge, the electron pressure ratio across the edge is 1.57 ± 0.69 , which is consistent with pressure equilibrium, especially if some amount of ram pressure exists.

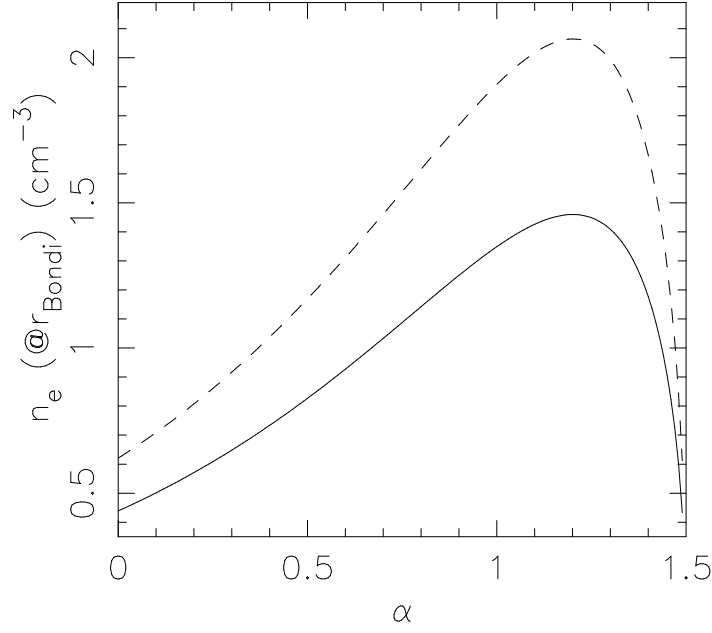


FIG. 8.— The electron density of ESO 137-006's gas at the Bondi radius (62 pc) vs. the slope of the density profile ($n_e \propto r^{-\alpha}$). The solid line is the relation for the observed normalization of the innermost bin. No PSF correction was done. When $\alpha=0$, the density goes back to the average value as shown in Fig. 7. The dashed line is for the relation when the normalization is doubled, which should over-estimate the PSF correction.

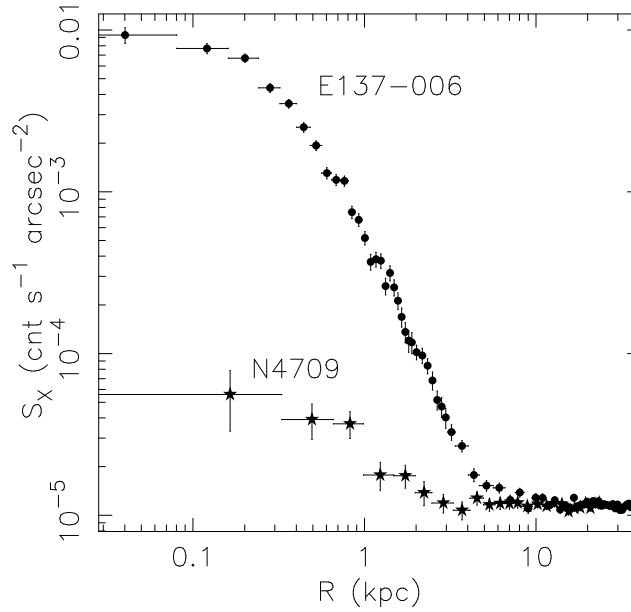


FIG. 9.— 0.5 - 2 keV surface brightness profiles of a faint embedded corona (NGC 4709) vs. a luminous embedded corona (ESO 137-006). Their local background has been matched to the same level. For NGC 4709's profile, the LMXB light is subtracted (with the assumption to follow the optical light) as it contributes half of the 0.5 - 2 keV emission. These two examples show that the embedded coronae have wide ranges of the X-ray luminosities (2×10^{39} ergs s $^{-1}$ to 2×10^{41} ergs s $^{-1}$), central densities (0.03 cm $^{-3}$ to 0.5 cm $^{-3}$) and gas masses ($0.02 - 2 \times 10^8 M_{\odot}$) (Table 4).

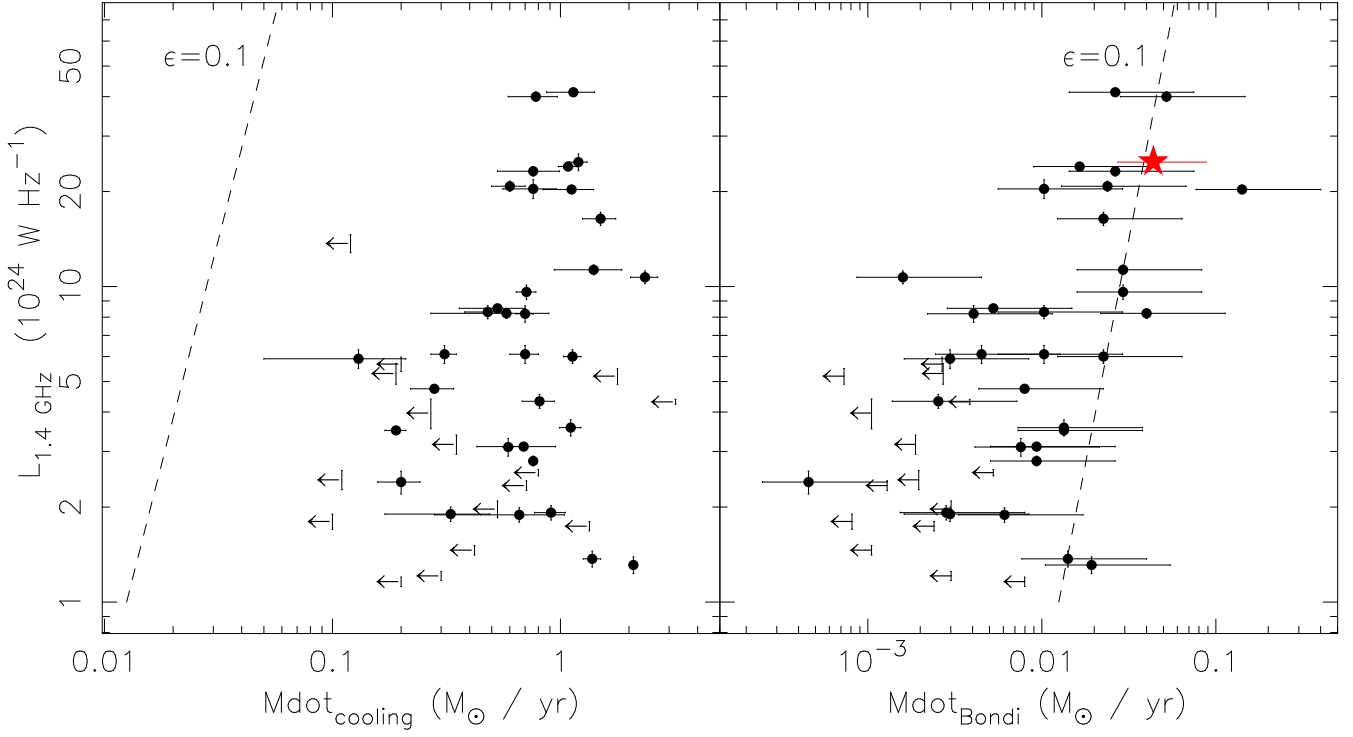


FIG. 10.— **Left:** the mass deposition rate from cooling (see §7.1) vs. the 1.4 GHz luminosity for coronae associated with strong radio AGN (i.e., the upper portion of the corona class, Fig. 1). The dashed line shows the required SMBH mass accretion rate to drive radio outflows for a mass-energy conversion efficiency of 10%. The relation between the radio luminosity and the mechanical power of the radio outflows is from Bîrzan et al. (2008), which has a large scatter and also likely under-estimates the mechanical power. This plot shows that in principle, only a small fraction of the cooled coronal gas is needed to provide enough fuel to power radio AGN. **Right:** the estimated Bondi accretion rate vs. the 1.4 GHz luminosity for coronae associated with strong radio AGN (see Section 7.1 for our assumption). The dashed line is the same as the one in the left plot. The red star is ESO 137-006. As discussed in Section 7.1, some luminous coronae of massive galaxies may be able to power their radio AGN through Bondi accretion.

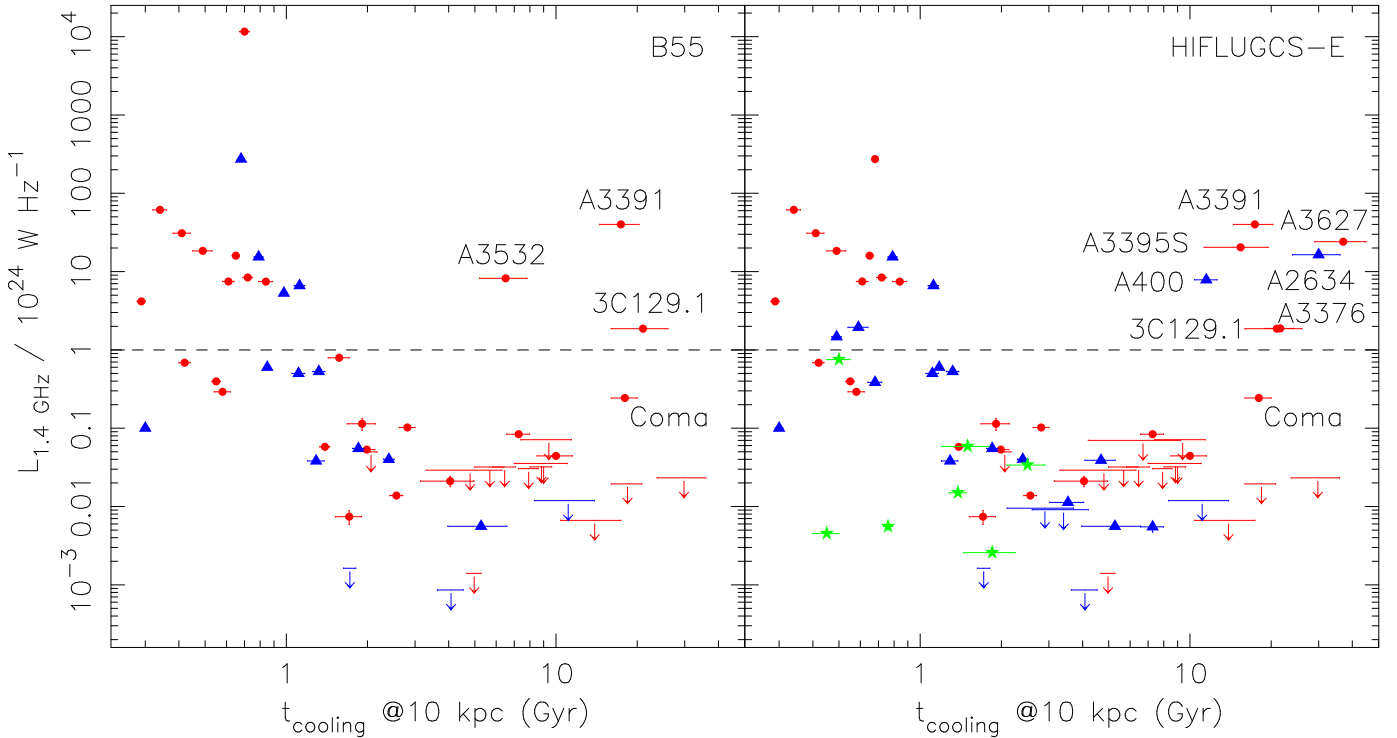


FIG. 11.— Cooling time at 10 kpc radius of the BCG vs. the 1.4 GHz luminosity of the BCG for the B55 and the extended HIFLUGCS samples (Section 7.4). Red points are $kT > 4 \text{ keV}$ clusters. Blue triangles are $kT = 2-4 \text{ keV}$ poor clusters, while green stars are $kT < 2 \text{ keV}$ groups. There is a general trend that strong radio AGN only exist in gas cores with short cooling time. However, there are three outliers in the B55 sample and seven outliers in the extended HIFLUGCS sample above $L_{1.4 \text{ GHz}}$ of $10^{24} \text{ W Hz}^{-1}$ (eight in total, all marked). All eight BCGs have coronae that are smaller than 10 kpc in radius. This again shows that BCGs with luminous radio AGN either host a large cool core or a small corona. BCGs of weak cool cores and noncool cores ($t_{\text{cooling}, 10 \text{ kpc}} > 2 \text{ Gyr}$) without a corona only have weak radio AGN (Coma have BCG coronae, Vikhlinin et al. 2001).